LEGIBILITY NOTICE

A major purpose of the Technical Information Center is to provide the broadest dissemination possible of information contained in DOE's Research and Development Reports to business, industry, the academic community, and federal, state and local governments.

Although a small portion of this report is not reproducible, it is being made available to expedite the availability of information on the research discussed herein.

Los Alamos National Laboratory is operated by the University of California for the United States Department of Energy under contract W-7405-ENG-36

LA-UR--90-1000

DE90 008918

TITLE DYNAMICS OF CAVITONS IN STRONG LANGMUIR TURBULENCE

AUTHOR(S) D. F. DuBois, T-DOT
Harvey A. Rose, T-DOT
David Russell, T-DOT

SUBMITTED TO Proceedings of Conference on Nonlinear and Relativistic Effects in Plasmas, La Jolla, CA February 5-8, 1990

DISCLAIMER

Los Alamos Los Alamos National Laboratory
Los Alamos, New Mexico 87545

Dynamics of Cavitons in Strong Langmuir Turbulence*

D. F. DuBois, Harvey A. Rose and David Russell
Theoretical Division and Center for Nonlinear Studies**
Los Alamos National Laboratory, Los Alamos, NM, 87545

Recent studies of Langmuir turbulence as described by Zakharov's model will be reviewed. For parameters of interest in laser-plasma experiments and for ionospheric HF heating experiments a significant fraction of the turbulent energy is in nonlinear "caviton" excitations which are localized in space and time. A local caviton model will be presented which accounts for the nucleation-collapse-burnout cycles of individual cavitons as well as their space-time correlations. This model is in detailed agreement with many features of the electron density fluctuation spectra in the ionosphere modified by powerful HF waves as measured by incoherent scatter radar. Recently such observations have verified a prediction of the theory that "free" Langmiur waves are emitted in the caviton collapse process. Observations and theoretical considerations also imply that when the pump frequency is slightly lower than the ambient electron plasma frequency cavitons may evolve to states in which they are ordered in space and time. The sensitivity of the high frequency Langmuir field dynamics to the low frequency ion density fluctuations and the related caviton nucleation process will be discussed.

**Research supported by USDOE.

I. INTRODUCTION

There are many linear instabilities in plasmas which result in the excitation of intense Langmuir waves. An important subgroup of such instabilities are the radiation-induced parametric instabilities which have been studied extensively since 1965.[1,2] In the last decade important progress has been made in understanding the nonlinear, and usually turbulent state to which these instabilities evolve. It has become increasingly clear that the older approaches involving weak turbulence theory, as one extreme, and the wave-breaking of traveling Langmuir waves, as another limit, are not adequate, especially on the longer time scales associated with ion motion. Instead, a new paradigm is emerging involving the concepts of what is commonly called strong Langmuir turbulence (SLT) theory. This theory has its roots in the seminal work of V. E. Zakharov[3] who developed a compact mathematical model of SLT and concluded that localized collapsing Langmuir states could play a central role in the turbulent state.

In recent years it has been possible to carry out long time computer solutions[4–8] of Zakharov's model equations, suitably modified to treat the effect of various types of driving sources. This research has led to a "global" view of how the turbulent state is sustained by the balance of driving sources and the dissipation resulting from the transfer of energy from the collapsing electrostatic fields to accelerated electrons.

The new paradigm has received support from various experiments including beam driven laboratory experiments,[9] laser-plasma experiments[10,11] and recently from detailed ionospheric modification experiments.[12] The power spectra of turbulent fluctuations measured by Thomson scatter radars from the modified ionosphere provides detailed information concerning the dynamics of the elementary excitations, the "cavitons" and the "free modes" which are important in SLT. An important part of the SLT scenario is the controlling effect of low frequency density fluctuations on the localization of the Langmuir fields. Laser-plasma experiments,[10,11] which demonstrated various aspects of the nonlinear coupling of stimulated Raman scattering (SRS) and stimulated Brillouin scattering (SBS), provided useful tests of the predictions[13] that the ion sound waves from SBS would have a controlling effect on the Langmuir waves from SRS. The temporal signatures of the Thomson scatter signals from these two types of fluctuations where consistent with the evolution to

collapse of the Langmuir waves in regimes where the levels of ion sound waves were low enough to permit the growth of intense Langmuir waves.

The research program at Los Alamos has concentrated on SLT driven by various radiation sources. These include the ponderomotive sources appropriate to SRS and SBS. Our most comprehensive studies have involved long wavelength electric field drivers with frequencies near the electron plasma frequency.[14] This method of driving is appropriate for the turbulence induced in the ionosphere, near the reflection density, by HF pump (or heater) waves of ordinary polarization. In a quiescent plasma such drivers can excite the well-known parametric decay instability[1] (PDI) or the modulational instability[15,16] (MI) (sometimes called the oscillating two stream instability.)

The results of this research on SLT driven near critical density can be summarized as follows:

1.) States of SLT can be excited for heater (pump) intensities only marginally above the threshold for parametric instabilities. Thus, for example, we expect the ionospheric heating experiments, which are estimated to be well above the threshold for these parametric instabilities will be in the SLT regime.

2.) In these states of SLT a significant part of the energy in high frequency density fluctuations is contained in localized states in the case of strong ion sound wave damping which is appropriate to the ionosphere.[4,5,14] These localized states, which we will call cavitons, consist of a high frequency Langmuir field trapped in a self-consistent density cavity (i.e., density depletion). The dynamics of these cavitons will be a major concern of this paper. It is important to emphasize that these localized states are not wavepackets of plane linear Langmuir waves, but new nonlinear Langmuir states and consequently cannot be described by perturbation arguments such as weak turbulence theory based on Langmuir wave states satisfying the linear dispersion relation.

3.) This state of SLT is sustained by a local nucleation process, (see 6. below), and not by linear parametric instabilities.[4,7,8] The developed turbulent state is stable to the excitation of these global parametric processes because of the level and localized nature of the turbulent fluctuations. Parametric instabilities may play a role in the transient excitation of the SLT state from quiescent initial conditions; for ionospheric parameters this would be the first ms following the turn-on of the heater.

4.) The localized states are trapped in self-consistently evolving density wells which collapse to small dimensions because of the dominance of the nonlinear ponderomotive force over the linear pressure force. The evolution from nucleation to collapse is discussed by Rose and Weinstein[17] and the collapse process follows the self-similar scaling discussed by several Soviet authors.[3,18]

5.) As the caviton's spatial dimension decreases to the order of 5-10 electron Debye lengths, λ_{De}, the electrostatic energy trapped in the caviton is rapidly given up in the acceleration of electrons resulting in the sudden dissipation or "burnout" of electrostatic energy. The interaction of cavitons by the exchange of hot electrons appears to be a weak effect. Even in regimes where there is significant energy in free modes (see (7.)) the burnout of cavitons is the dominant source of energy dissipation.

6.) The electrostatic burnout process leaves an empty density cavity, no longer supported by a ponderomotive force, which then evolves as a free, possibly nonlinear, ion sound pulse. These residual ion density wells provide nucleation centers for the excitation of new collapsing cavitons.[4,7,8] For strong ion sound damping, the burntout density wells relax in place. The radiation of ion sound waves following collapse is an important interaction mechanism for cavitons.

7.) The collapsing cavitons emit and absorb propagating Langmuir waves.[14] This provides another interaction mechanism for cavitons. Under some conditions the free mode-caviton interaction may be an important source driving caviton nucleation. The free modes generated by collapse have been observed in ionospheric heating.[12] These free modes can interact with one another by familiar wave-wave processes. They also can influence the nucleation of localized states.

8.) When the driving frequency exceeds the background plasma frequency, i.e. for overdense driving, the caviton cycles of nucleation-collapse-burnout can become stable limit cycles.[14] Under some conditions the cavitons can also settle into stable periodic spatial patterns. These ordered states of high spatio-temporal correlation have distinct signatures in the power spectra of the turbulent fluctuations.

Highlights of this research have been reported in several short articles.[4,5,7,8] A longer article, ref. 14, is devoted mainly to the regime of ionospheric heating which greatly reduces the "volume" of the potentially very large parameter space of SLT which is considered, although what remains is still very rich in phenomena.

Other applications such as laser-plasma interactions (e.g., see Rose, DuBois and Bezzerides[13,19]) involve many of the same or related phenomena and will be mentioned here briefly. The same conditions of excitation near the critical density in weak density gradients as considered for ionospheric heating might be approximated in long scale length laser produced plasmas with weak collisionality or in laboratory microwave-plasma experiments with sufficiently long-lived plasmas uneffected by boundaries. We will not treat such applications in detail here.

Here we will try to sketch out the major features of this strong turbulence scenario. The physical setting of HF heating of the ionosphere is ideal for observing SLT phenomena. We believe the SLT theory represents the most credible description of the experimental facts of ionospheric heating. This SLT approach represents a significant departure from the accepted or conventional ideas associated with parametric instabilities and weak turbulence cascades. Our most complete current understanding of SLT is based on simulations of a homogeneous, isothermal model described by Zakharov's equations.[3] This situation is best realized in ionospheric modification for early times (several ms) after heater turn on before large scale (several m) density and temperature fluctuations have had time to develop.

A more detailed comparison of the SLT theory to ionospheric modification experiments is given in reference 14.

2. ZAKHAROV'S MODEL OF NONLINEAR LANGMUIR WAVE-ION SOUND WAVE INTERACTIONS

The calculations to be reported here are based on solutions of Zakharov's model[3] of Langmuir wave-ion sound wave interactions. These are formulated in terms of the slowly time varying envelope field $\underline{E}$ (x,t) of the total electrostatic field $\underline{E}_{TOT}$ (x,t), where

$$\underline{E}_{TOT}(\underline{x},t) = \frac{1}{2}\underline{\tilde{E}}(\underline{\tilde{x}},\tilde{t})exp[-i\omega_p\tilde{t}] + c.c \qquad (2.1)$$

where $\omega_p^2 = 4\pi e^2 n_0/m_e$ where n_0 is the mean plasma electron density. It is assumed that

$$|\tilde{\partial}_t\underline{\tilde{E}}| << |\omega_p\underline{\tilde{E}}| \, . \qquad (2.2)$$

The total ion density is written as

$$n_{TOT} = n_0 + \tilde{n} \tag{2.3}$$

where $\tilde{n}$ is the fluctuation about the mean density; the spatial average of $\tilde{n}$ is then zero.

The equations of Zakharov's model are:

$$\underline{\nabla} \cdot \left[i(\tilde{\partial}_t + \tilde{\nu}_e \bullet) + \frac{3}{2}\, \omega_p \lambda_D^2 \tilde{\nabla}^2 - \frac{1}{2}\, \frac{\tilde{n}}{n_o}\, \omega_p \right] \underline{\tilde{E}} = \underline{\tilde{E}}_0 \cdot \underline{\nabla} \left[\frac{\tilde{n}}{2n_0}\, \omega_p \right] \tag{2.4a}$$

$$\left[\tilde{\partial}_t^2 + 2\tilde{\nu}_i \bullet \tilde{\partial}_t - c_s^2 \tilde{\nabla}^2 \right] \tilde{n} = \frac{1}{16\pi m_i}\, \nabla^2 |\underline{\tilde{E}} + \underline{\tilde{E}}_0|^2 \tag{2.4b}$$

where $\underline{\nabla}$ x $\underline{\tilde{E}} = 0$. Here λ_D is the electron Debye length and $c_S = (\eta\ T_e/m_i)^{1/2}$ is the ion acoustic speed which is often expressed in terms of specific heat parameters. $\underline{\tilde{E}}_0$ is the possibly time-dependent pump which is assumed to be spatially uniform. This is the "heater" field in ionspheric modification experiments. Tildes are used to denote conventional dimensional quantities to distinguish them where necessary from dimensionless quantities introduced below.

The damping operators $\tilde{\nu}_e \bullet$ and $\tilde{\nu}_i \bullet$ which are nonlocal in coordinate space are local in Fourier space. In Fourier space it is also simple to include a weak background geomagnetic field $\underline{B}_0$based on the modified Bohm-Gross dispersion relation for Langmuir waves.[14,20]

$$\omega(k)^2 = \omega_p^2 + 3k^2 v_e^2 + \omega_c^2 sin^2\ \theta \tag{2.5}$$

where $v_e^2 = T_e/m_e$, $\omega_c = e\ B_o/mc$ and θ is the angle between $\underline{B}_o$ and $\underline{k}$.

In this paper we adopt the convention for spatial Fourier transforms:

$$E(\underline{k}) = (L)^{-D} \int d^D x\ exp[-i\underline{k} \cdot \underline{x}] E(\underline{x}) \tag{2.6}$$

where L is the linear dimension of the system and D is the dimensionality of space.

The ionospheric heater or "pump" field $\underline{\tilde{E}}_0(t)$ is included, ignoring pump depletion, by assuming that the spatially uniform, k = 0, Fourier component is a given function. We will generally take $\underline{\tilde{E}}_0(t)=\underline{\tilde{E}}_0 \exp[-i\tilde{\omega}_0 t]$ where $\tilde{\omega}_0=\omega_H-\omega_p$ is the difference between the heater (or pump) frequency and the average plasma frequency.

The Langmuir wave dumping term is taken to be collisional damping plus Landau damping.

$$\tilde{\nu}_e(\tilde{k})/\omega_p = \tilde{\nu}_c/\omega_p + \sqrt{\pi}/8e^{-3/2}(k_D/\tilde{k})^3 exp - (k_D^2/2\tilde{k}^2) \qquad (2.7)$$

for $\tilde{k} < 0.3k_D$; this function is continued smoothly to increase as $\tilde{k}^2$ for large $\tilde{k}$. The latter step is necessary in order to arrest collapse at small scales as discussed by Zakharov and Shur[21] and Russell et al.;[4,8] it is essential for numerical resolution. This damping is an ad hoc addition to the model which is justified by comparing with particle in cell simulations[22–25] which show nearly complete dissipation of the trapped electrostatic field at the burnout stage of collapse. For the work reported here, where we treat heater intensities well above the collisional thresholds for parametric instabilities, we will take $\tilde{\nu}_c = 0$. This is valid provided all physically important rates are much larger than $\tilde{\nu}_c$.[14]

For ionospheric conditions we expect the ratio of electron to ion temperatures, T_e/T_i, to be of order unity for early times after the onset of heating. Fluid description of the ion density response is then expected to be quantitatively inaccurate because of the important role of Landau damping on ions.[26] Since kinetic simulations of the ion response are prohibitively expensive for the problems we treat here we have adopted the following strategy: We use the fluid description of (2.4b) but the sound velocity c_S and the ion Landau damping used in this equation are chosen to coincide with the least damped poles of the linear kinetic response. Using this procedure we find for $\tilde{k} << k_{D_e}$ that $\tilde{\nu}_i(\tilde{k})/\tilde{\omega}_i(\tilde{k}) = \nu_i$ where $\tilde{\omega}_i(k) = \tilde{k}(\eta\ T_e/m_i)^{1/2}$. The values of ν_i and η are found from the least damped roots of the full kinetic dispersion relation.[14]

We have found the qualitative features of the nucleation process to be unaffected by the values of ν_i in the regime $0.9 > \nu_i > 0.4$ for systems driven well above the nucleation threshold discussed in Sec. 3.

It is well-known,[3] that the linearized form of these equations contains the parametric decay instability (PDI)[1] and modulational instability[15,16] (MI or OTSI) of the pump wave. Furthermore, when weak turbulence analysis[27,28] is applied to these equations it yields the usual wave kinetic type of equations which lead to the weak turbulence cascade. However, the validity conditions for the weak turbulence approximations are very limiting.[28]

We have studied examples of the solution of these equations for parameters relevant to ionosphere heating in which the system is initially excited by a linear parametric instability and evolves to a state of SLT.[14] In this paper, however, we will consider only the developed turbulent state.

In carrying out numerical solutions of these equations it is convenient to use dimensionless untilded quantities which are related to dimensional tilded quantities in the following way:[27]

$$t \equiv \frac{2}{3}\left(\eta\frac{m_e}{m_i}\right)\omega_p\tilde{t}$$

$$x \equiv \frac{2}{3}\left(\eta\frac{m_e}{m_i}\right)^{1/2}\frac{\tilde{x}}{\lambda_D} \tag{2.8}$$

$$E = \frac{1}{\eta^{1/2}}\left(\frac{m_i}{\eta m_e}\right)^{1/2}\left(\frac{3}{16}\,\frac{\tilde{E}^2}{4\pi n_0 T_e}\right)^{1/2}$$

$$\eta = \frac{3}{4}\left(\frac{m_i}{\eta m_e}\right)^{1/2}\frac{\tilde{n}}{n_o}$$

The scaled equations then have the familiar simple form

$$\underline{\nabla}\cdot[i(\partial_t + \nu_e\bullet) + \nabla^2 - n]\underline{E} = \underline{E}_0\cdot\underline{\nabla}n + S_R \tag{2.9a}$$

$$[\partial_t^2 + 2\nu_i\bullet\partial_t - \nabla^2]n = \nabla^2|\underline{E} + \underline{E}_0|^2 + S_B \tag{2.9b}$$

In the scaled units there is a residual mass ratio dependence which occurs only in the scaled damping rate which is obtained from (2.7) as follows:

$$\nu_e(k) = (3/2)M\tilde{\nu}_e(2/3M^{-1/2}kk_D)\omega_p^{-1} \qquad (2.10)$$

in terms of the scaled wavenumber k and $M = m_i/\eta m_e$. This residual mass ratio dependence reflects the ratio of the parametric instability space and time scales which increase with M and the mass ratio independent dissipation scale. A similar formula applies to $\nu_i(k)$.

Here we have added source terms S_R and S_B in (2.9a) and (2.9b) which arise when the turbulence is driven by the SRS interaction and the SBS interaction, respectively. We will not give the specific formulae here but refer the reader to ref. 13.

Note that in dimensional units Landau damping becomes significant for $\tilde{k} > 0.2k_D(k_D = \lambda_D{}^{-1})$. Thus in dimensionless units this dissipation becomes significant for k greater than the dissipation scale k_d:

$$k > k_d \simeq (0.2) \cdot \frac{3}{2}\left(\frac{m_i}{\eta m_e}\right)^{1/2}$$

Since the dynamics of the decay instability involves $\tilde{k}$'s on the scale of $\tilde{k}_* = (2/3)(\eta m_e/m_i)^{1/2}\, k_D$ we need Fourier components at <u>least</u> as small as this, if the parametric processes are important, and this sets the linear dimension of the simulation cell to be $\tilde{L}_x = \tilde{L}_y > 2\pi/k_*$. In dimensionless units $k_* = 1$ and $L_x = L_y > 2\pi$. The number of Fourier modes must be sufficient to probe deep within the dissipation range of $k_{max} >> k_d$ in order to resolve collapse. This sets a limit on the value of M which can be accommodated in a reasonably sized simulation of say 128 × 128 Fourier modes in two dimensions. In view of these limitations we have chosen M = 1836 for our simulations. In ref. 14, Section 3, we discussed the scaling of physical quantities with the mass ratio. This scaling allows us, at least roughly, to translate the simulation results to the larger mass ratios.

The validity conditions for Zakharov's model have been discussed elsewhere[3,27] and include the condition.

$$\frac{|\tilde{E}|^2}{4\pi n_0 T_e} << 1 \qquad (2.11a)$$

$$\frac{\tilde{n}}{n_0} << 1 \qquad (2.11b)$$

A discussion of the degree to which these conditions are satisfied in our numerical simulations is given in reference 14.

Our simulations are carried out on a 128 × 128 square grid of sides $L_x = L_y = 2\pi$, with periodic boundary conditions in x and y. In physical units this implies $L_x = L_y = 404\ \lambda_{D_e}$ and a grid-point spacing $\Delta x = \Delta y = 3.15\ \lambda_{D_e}$. The Debye wavenumber in these units is 64.3 and the maximum wavenumber is 91. Spot checks with a dealiased code with a nominal 256 × 256 grid were used to confirm the validity of our simulations. Typically the spectrum $\langle|n(k)|^2\rangle$ decreases by 4 orders of magnitude between the k values for which the spectrum peaks and the largest k values. The test of temporal and spatial resolution is energy conservation as expressed by the balance between the average dissipation and injection rates.[14]

3. THE LOCAL CAVITON MODEL

The accumulated evidence from many computer simulations of equations (2.4) shows that, at least for moderate to strong ion acoustic wave damping, $\nu_i \gtrsim 0.1$, the strongly turbulent system is dominated by caviton "events" which are localized in space and time. Snapshots such as Figure 1 show the localized nature of $|\underline{E}(\underline{x},t)|^2$ and $n(\underline{x},t)$ as functions of $\underline{x}$ for given t. The power spectra $|\underline{E}(\underline{k},\omega)|^2$, which we will discuss in detail below, also have signatures of localized states. The envelope field $\underline{E}(x,t)$ in this case can be modeled by a sum over events i:

$$\underline{E}(x,t) = \sum_{i=0}^{N(t)} \hat{\underline{\varepsilon}}_i(\underline{x} - \underline{x}_i, t - t_i) + \underline{E}_{nonlocal}(\underline{x},t) \qquad (3.1)$$

Here a caviton event i is localized at the space time point $\underline{x}_i$, t_i. The single event function $\hat{\underline{\varepsilon}}_i(\underline{x},t)$ has its maximum at x=0, t=0 with a spatial width $\underline{\delta}_i(t)$ and a temporal width or lifetime τ_i; from the simulations we find this lifetime to be of the order of 0.05 to 0.1 ms for ionospheric parameters. At a given time t, the number of events N(t) which contribute to the sum in (3.1) are those for which $0< |t-t_i| < \tau_i$ which is clearly proportional to the volume of the system if the cavitons are roughly uniformly distributed. For example, if the portion of the heated volume observed by

the radar is ionospheric heating experiments is $(200\ \mathrm{m})^3$, the mean caviton spacing is 0.25 m which is about 50 λ_{De} as observed in our simulations, and accounting for the time scales of the caviton cycles as observed in simulations, we find $N(t) \sim 10^7$ which is crude but representative. In (3.1) the term $\underline{E}_{nonlocal}(\underline{x},t)$ represents the nonlocalized or free mode part of the envelope field which is relatively negligible for systems driven with heater (or pump) frequencies near or slightly below the ambient electron plasma frequency.

This local caviton model can be put into a more formal setting by introducing the instantaneous vector eigenfunctions $\underline{e}_\nu(\underline{x},t)$ of the operator on the left hand side of (2.9a). These satisfy (for $B_0 = 0$)

$$\underline{\nabla} \cdot \left[\lambda_\nu(t) + \nabla^2 - n(\underline{x},t)\right] \underline{e}_\nu(\underline{x},t) = 0 \tag{3.2}$$

where $\lambda_\nu(t)$ is the corresponding instantaneous eigenvalue and $\underline{\nabla}$ x $\underline{e}_\nu = 0$. These are nothing more than the Langmuir modes in a nonuniform density background. In ordinary units this can be written as

$$\underline{\nabla} \cdot \left[\omega_\nu - \omega_p(x,t) \ + \ \frac{3}{2}\ \lambda_D^2 \omega_{po}\ \nabla^2\right] \underline{e}_\nu(\underline{x},t) = 0 \tag{3.3}$$

where

$$\omega_p(x,t) = \omega_{p_0}\left(1 + \frac{1}{2}\ \frac{n(xt)}{n_0}\right)$$

is the spatially fluctuating plasma frequency. Thus we can relate λ_ν in scaled units to ω_ν in ordinary units:

$$\lambda_\nu(t) \ = \ \frac{\omega_\nu - \omega_{p_0}}{\omega_{p_0}} \ \cdot \ \frac{2}{3}\left(\frac{m_i}{\eta m_e}\right)^{1/2} \tag{3.4}$$

The complete description of these states for an arbitrary $n(\underline{x},t)$, especially for $D \geq 2$ is beyond our capability. In $D = 1$ it is relatively easy to compute these states from an arbitrary realization of $n(x,t)$ obtained from the complete numerical simulation of (2.9a,b).[7]

The form of the density fluctuation field $n(x,t)$ can have a profound effect on the eigenstates of the Langmuir field. Most importantly, some of these states are

localized in a density minimum (i.e. depressions). Roughly the condition for a localized state to occur in a density depression $\tilde{n}$ ($\tilde{n}$<o) and spatial extent $\tilde{\delta}$ is

$$\left|\frac{\tilde{n}}{n_o}\right|\left(\frac{\tilde{\delta}}{\lambda_D}\right)^2 \simeq O(1)$$

which can be satisfied for example for $|\tilde{n}/n_o| \sim 10^{-3}, (\delta/\lambda_D) \sim 30$. This condition is similar to the conditions on the depth and width of a potential well which can sustain a bound state of the Schroedinger equation of quantum mechanics. The density wells which trap these localized states might arise from initial background density fluctuations, from density wells remaining from earlier collapse events or from density fluctuations driven by some instability such as SBS.

In the case of SBS-generated ion sound waves, we can sometimes regard these density fluctuations as being periodic in space with a wavelength corresponding to the fastest growing SBS mode. The eigenstates $\underline{e}_\nu(x,t)$ in this case can be regarded as one dimensional Bloch waves with lattice wave vector $\underline{k}$ and with eigenvalues $\lambda_{\underline{k},\nu}(t)$ which lie in bands, labelled by the index ν, just as in solid state physics.[29,13] As the periodic density fluctuation grows exponentially in time due to the SBS instability the Langmuir mode eigenfuctions $\lambda_{\nu k}(t)$ change in time. If a stimulated Raman instability is simultaneously excited, the SRS frequency matching condition, $\Delta\omega = \omega^{laser}_{\underline{k}_o} - \lambda_{\underline{k},\nu}(t) - \omega^{scatteredlight}_{\underline{k}_o - k} = 0$, can only be satisfied instantaneously for a given Langmuir Bloch mode with lattice wave vector $\underline{k}$. In fact if $\left|\frac{d\Delta\omega}{dt}\right| = \left|\frac{d}{dt}\lambda_{k,\nu}\right| > \gamma_R^2$, where γ_R is the instantaneous SRS growth rate, then it can be shown[13,29] that the SRS instability is <u>detuned</u> by the growing SBS ion sound wave and SRS is suppressed. Experiments carried out at the NRC Laboratory in Canada[10,11] appear to be consistent with this scenario. The experiment by Villeneuve et al.[11] verified the theoretical prediction[13] that a "seeded" SBS instability could suppress SRS. In other parameter regimes where SRS is not suppressed the (weaker) SBS ion sound wave may still impose its spatial periodicity on the SRS Langmuir eigenfunctions.[13] These envelope eigenfunctions have a periodic array of maxima of $|\underline{E}|^2$ (or $|\underline{c}_{k,\nu}|^2$) which have a finite ponderomotive force (PMF). This periodic PMF causes a periodic array of density wells to develop in which the Langmuir waves are trapped and can be driven to collapse. [Note the ponderomotive driven periodic density wells do not coincide in general with the density minima of the SBS sound waves but they have the same periodicity.] In Fig. 2, taken from ref.

13, we show typical spatial configurations of $|E|^2$ and n, before and after collapse and burnout.

The impulsive time signature of the Thomson-scattering signal from Langmuir fluctuations in the experiment of Walsh et al.,[10] is consistent with the collapse of SRS driven Langmuuir fluctuations. The large ion density fluctuations remaining from the burntout cavitons then act as seeds for the subsequent strong SBS pulse. In Fig. 2 the time signatures of the Langmuir and ion sound fluctuations, obtained from numerical solutions of the SRS-SBS driven Zakharov equations, are shown. Further evidence consistent with the controlling effect of SBS generated ion sound waves on the SRS process is found in the experiments of Baldis et al.[30]

The electric field envelope of the Zakharov equations (2.9a,b) can be resolved in the complete set of states $\underline{e}_\nu(\underline{x},t)$:

$$\underline{E}(x,t) = \sum_\nu h_\nu(t)\underline{e}_\nu(\underline{x},t)exp(-i\omega_0 t) \tag{3.6}$$

(In an infinite system the sum may imply an integral over continuum states.) The equation of motion for the amplitudes $h_\nu(t)$ is readily found from (2.9a) to be

$$i\dot{h}_\nu(t) + (\omega_0 - \lambda_\nu(t)h_\nu(t) + i\sum_{\nu\prime}\left[\langle \underline{e}_\nu \blacklozenge \nu_e \underline{e}_{\nu\prime}\rangle + \langle \underline{e}_\nu \blacklozenge \dot{\underline{e}}_{\nu\prime}\rangle\right] h_{\nu\prime} = \underline{E}_0 \cdot \langle \underline{e}_\nu | n\rangle \tag{3.7}$$

Here we have taken the $\underline{e}_\nu$ to be a complete orthonormal set with

$$\langle \underline{e}_\nu \blacklozenge \underline{e}_{\nu\prime}\rangle = \int d\underline{x}\underline{e}^*_\nu(\underline{x},t)\cdot \underline{e}_{\nu\prime}(\underline{x},t) = \delta_{\nu\nu\prime} \tag{3.8}$$

and have used the notation

$$\langle \underline{e}_\nu \blacklozenge \dot{\underline{e}}_{\nu\prime}\rangle = \int d\underline{x}\ \underline{e}^*_\nu(\underline{x},t)\cdot\frac{d}{dt}\underline{e}_{\nu\prime}(\underline{x},t) \tag{3.9a}$$

$$\langle \underline{e}_\nu \blacklozenge \nu_e \underline{e}_{\nu\prime}\rangle = \int d\underline{x}\int d\underline{x}'\underline{e}_\nu(\underline{x},t)\cdot\nu_e(\underline{x}-\underline{x}')\underline{e}_{\nu\prime}(\underline{x}',t) \tag{3.9b}$$

$$\underline{E}_0\cdot\langle \underline{e}_\nu|n\rangle = \underline{E}_0\cdot\int d\underline{x}\ \underline{e}^*_\nu(\underline{x},t)n(\underline{x},t) \equiv S_0 \tag{3.9c}$$

To understand the various terms in (3.7) first consider the case where $n(\underline{x})$ is independent of time and therefore $(d/dt)\,\underline{e}_\nu(\underline{x}) = 0$. Then the amplitude h_ν is driven directly by the source term $\underline{E}_0 \cdot \langle\, \underline{e}_\nu | n \,\rangle$. If $\underline{e}_\nu$ were a plane wave state proportional to exp i $\underline{k}\cdot\underline{x}$; then this source term is proportional to $\underline{E}_0 \cdot \underline{k}\; n(\underline{k})$ the so called direct conversion source term.[14,31] However, the important states are the localized states. The coefficient $\langle\, \underline{e}_\nu \,\phi\, \nu_e\, \underline{e}_{\nu\prime} \rangle$ couples states because of the nonlocal nature of the Landau damping. This term becomes important in the time dependent case only in the burnout phase. Note that by introducing the spatial Fourier transform of the eigenstates $\underline{e}_\nu(k,t)$ we can write

$$\langle \underline{e}_\nu \,\phi\, \nu_e \underline{e}_{\nu\prime} \rangle \;=\; \sum_{\underline{k}} \underline{e}^*_\nu(\underline{k},t) \cdot \underline{e}_{\nu\prime}(\underline{k},t)\nu_e(\underline{k}) \tag{3.10}$$

For $\nu{=}\nu'$ this certainly becomes important in the burnout phase. For $\nu \neq \nu'$ this is less important if one of the states is not localized - e.g., noncollapsing - or is localized at a different space-time point.

In the time-dependent case of interest the coefficient $\langle e_\nu \,\phi\, \dot{e}_{\nu\prime} \rangle$ can provide a coupling between rapidly collapsing states, say ν' and a nonlocalized state ν. This is one of the mechanisms responsible for the excitation of the "free mode" states observed in the spectra. We will return to this detail below.

We note that a subset $\{i\}$ of the states $\{\nu\}$ are localized at $x{=}x_i$ in density depressions of $n(\underline{x},t)$ and some of these, which have the proper symmetry to couple to the pump $\underline{E}_0$, evolve to collapse. This subset of states can be viewed as local ground states of the "potential" $n(\underline{x},t)$.

We can now make a tentative connection between the localized event functions $\underline{\xi}_i\,(\underline{x} - \underline{x}_i,\, t - t_i)$ of (3.1) and the subset $\{i\}$ of localized eigenstates. It is reasonable to identify

$$\underline{\xi}_i(\underline{r} - \underline{r}_i, t - t_i) = \underline{\varepsilon}_i(\underline{r} - \underline{r}_i, t - t_i) exp(-i\omega_0 t) \tag{3.11a}$$

where

$$\underline{\varepsilon}_i(\underline{r} - \underline{r}_i, t - t_i) \;=\; h_i(t)\underline{e}_i(\underline{r},t) \tag{3.11b}$$

The contributions from the remaining nonlocalized states in the set $\{\nu\}$ make up the term $\underline{E}_{nonlocal}$ (x,t) in (3.1).

The eigenstates $\underline{e}_i(\underline{x},t)$ are in a sense the natural basis or coordinates for describing the turbulent system. Unfortunately, they can only be obtained by first solving (2.9) for $n(\underline{x}.t)$. In spite of this they are conceptually useful and some observed properties of the turbulence can be related to general properties of these states. In effect the use of the states $\underline{e}_i(\underline{x},t)$ represents a huge reduction in the effective dimensionality of the problem. While we use $(128)^2$ Fourier modes for the simulation there may be of the order of 10 collapse sites in the cell and therefore roughly 10 localized states.

We have gained useful insight into the nature of these eigenstates and their connection to the observed turbulence by considering the <u>scalar</u> Zakharov model. In this model E(r,t) and E_0 are scalar fields and in place of (2.9) we have

$$\left[i(\partial_t + \nu_e \bullet) + \nabla^2 - n(\underline{x},t)\right] E(\underline{x},t) = E_0 n(\underline{x},t) \qquad (3.12a)$$

$$(\partial_t^2 + 2\nu_i \bullet \partial_t - \nabla^2) n(\underline{x},t) = \nabla^2 |E_0 + E(\underline{x},t)| \qquad (3.12b)$$

In this model only spherically symmetric collapsing cavitons are allowed and the three dimensional problem for an isolated collapse reduces to one in which E and n depend only on the radial coordinate r. This scalar model has several properties in common with the physical three-dimensional vector model (2.9): threshold and maximum growth rate for the modulational instability, collapse scaling exponents which are discussed below, no threshold energy for collapse and the possible failure of a density well to support a localized eigenstate.

Spherical symmetry is imposed by representing all fields in terms of the Fourier modes $\sin(k_\ell r)$, $k_\ell = \pi\ell/r_0$, $\ell = 1,2,--$, with r_o chosen large compared to a typical caviton size. In these scalar studies we have observed for $\nu_i(k)/k = 0.9$ that at the nucleation site, E(r,t) is dominated by its projection, $h_0(t)$, on the localized ground state $e_0(r,t)$. In nucleation $e_0(r,t)$ remains localized; at every time step $e_0(r,t)$ can be computed from n(r,t). Here we will adopt a simplified model in which $h_0(t)$ is evolved neglecting the excited state contributions $\nu' \neq 0$ in (3.7). The density evolves according to (3.12b) with the ponderomotive force replaced by $\nabla^2|E_0 +$

$h_0(t)e_0(r,t)|^2$. The solution to this model is insensitive to boundary conditions (i.e., the choice of r_0).

Let us restrict our attention to the case where ν_i is large enough so that after burnout, the relaxing density fluctuation is essentially nonpropagating. Immediately after burnout, energy absorption is minimal because the eigenvalue is large and negative, implying a far from resonant coupling to S_0 (see (3.9c)). The ponderomotive force is negligible, and the density fluctuation evolves according to the acoustic Green's function. A simple model for this phase of the dynamics is obtained by replacing the rhs of (3.12b) by $I\delta(t)\ \nabla^2\delta^3(\underline{x})$, where the "impulse" $I \equiv \int dt \int d\underline{x}|\varepsilon(\underline{x},t)|^2 = \int |h_0(t)|^2\ dt \approx \langle|h_0|^2\rangle\tau$. In three dimensions, the response of n is

$$n(x,t) \;=\; I \cdot G(|x|/t)/t^4 \qquad (3.13a)$$

where

$$G(\rho) \;=\; \frac{\nu_i}{\pi^2\rho}\,\frac{d^2}{d\rho^2}\left[\frac{\rho}{(1+\rho^2)^2 - 4\rho^2(1-\nu_i^2)}\right] . \qquad (3.13b)$$

Even though n is evolving self similarly, $\underline{e}_0$ is not. The figure of merit, μ, for the ground state is simply expressed in terms of the width w, $w(t) \sim t$, of n, and its depth, d, $d \sim I/t^4$, as $\mu \sim dw^2 \sim I/t^2$. If μ is too small, there is no localized state. Since 3D solitons are unstable, as t increases, either enough energy will be accumulated so that another collapse follows, or the bound state will be lost. In the latter case, the bound state will be localized in the immediate vicinity of the expanding density fluctuation, until just before the bound state is lost. So that during the time when energy is being injected, one may be able to ignore the coupling between states localized at different collapse sites. At a particular collapse site there is a lowest lying localized state which has a nonzero source. Excited states at the same site typically have a smaller source term because they are oscillatory while $\underline{E}_0\ n(\underline{x},t)$ is essentially uniform in direction. Also at a particular site there may only be a small number of localized states. This motivates the study of a model for the evolution of a caviton in a previously existing density fluctuation a process we call caviton nucleation - in which only one localized state is present. For a given ion fluctuation the lowest lying state, $\underline{e}_0$, with nonvanishing source, S_0,

(we shall call it the ground state) is calculated from (3.9c), h_0 is evolved according to (3.7) without the coupling to other amplitudes.

In Figure 3 we show some typical results from the scalar model driven by a spatially uniform field E_0 at the plasma frequency ($\omega_0 = 0$). For a range of E_0, a stable nucleation cycle is observed, with a complete cycle over the interval $0<t<t_c$. We expect that in a turbulent environment of other such nucleation sites, the strict periodicity of this cycle may be lost, but at a given site there may be strong correlations over a few cycle times for strong ion acoustic damping.

In fact, for overdense drive where the drive frequency ω_H is less than the background plasma frequency ω_p, i.e. for $\omega_o < o$, we have found[14] that over a range of driving amplitudes and ion wave damping strengths, ν_i, these cycles become stable limit cycles.

This is easily understood from the nucleation picture: For $\omega_0 < 0$ the relaxing density well remaining from a previous burnout comes earlier into resonance with the pump and therefore at a relatively deeper depletion compared to the $\omega_0 = 0$ case. Thus at the time of closest resonance $\lambda_\nu \sim \omega_0$ the eigenfunction $\underline{e}_\nu(\underline{x},t)$ is more confined. The caviton cycle presumably will be more stable and less effected by neighboring cavitons in this more confined caviton cycle. We expect more rapid caviton cycles, i.e , smaller τ_c, with less energy carried into collapse and this is verified by simulations. The overdense drive $\tilde{\omega}_0 < 0$ is much more efficient in the nucleation of cavitons.

An important observation of the scalar, local caviton model discussed in Section 3, is that the single event functions $\hat{\underline{\varepsilon}}_i(\underline{x} - \underline{x}_i, t - t_i)$ are phase locked to the pump. Thus it was more convenient to replace these functions in (3.1) by $\exp - i\omega_0 t$ $\hat{\varepsilon}_i(\underline{x} - \underline{x}_i, t - t_i)$; that is to explicitly separate out the pump phase. [See also (3.11).] Another way to look at the problem is to rewrite (2.9) in terms of $\hat{E}(\underline{x},t = \exp($ $- i\omega_0 t)\, E(\underline{x},t)$, i.e., to envelope around the pump frequency. As an equation for $\hat{E}$ the equations are autonomous, i.e., the drive term has no explicit time dependence but an additional term, $\omega_0\, \underline{\hat{E}}(\underline{k},t)$, appears on the left hand side of (2.9a). The result of this is that the single caviton spectra for $\omega_0 \neq 0$, $|\underline{\hat{\varepsilon}}(\underline{k},\omega)|^2$, have their spectral energy mainly for $\omega < \omega_0$. The eigenvalue trajectories versus time have the property that they reverse near the resonance $\lambda(t) \leq \omega_0$ where the PMF reverses the relaxation of the density well.

In Figure 4 we show snapshots of the lowest two eigenstates $e_0(r,t)$ and $e_1(r,t)$ and the density $n(r,t)$ as they evolve during one of these cycles for a case where $\omega_0 < 0$. In Figure 3a we show the time evolution of $|E(r = 0,t)|^2$ and $n(r=0,t)$, in Figure 3b the ground state eigenvalue $\lambda_0(t)$, the velocity Φ_0 of the phase of the amplitude $h_0(t) = |h_0(t)| \exp i\Phi_0(t)$, and in Figure 3c the electrostatic energy in the caviton $|h_o(t)|^2$. At the beginning of the cycle, t=0, the deep density well is relaxing from the previous burnout. From Fig. 3a we see that the peak $|E|^2$ occurs at about t=0.22 followed by its rapid burnout due to dissipation. The density well reaches its maximum depth shortly after at $t \simeq 0.235$. The maximum spatial extent of the eigenfunction $\delta(t)$ occurs earlier at $t \simeq 0.15$ which is also the time at which the well depth, $n(r=0,t)$, is shallowest. The well then deepens under the action of the PMF increasing the confinement of the eigenfunction. The eigenvalue $\lambda_o(t)$ approaches the pump frequency $\omega_0 = 0$, this causes a rapid increase in $|h_0(t)|^2$ as the mode frequency approaches resonance with the pump frequency. This rapidly increases the PMF and as the density well deepens again $\lambda_0(t)$ again decreases rapidly during collapse. This illustrates what we believe to be the typical behavior: As the relaxing density well becomes shallower and broader its eigenvalue approaches resonance with the pump causing a rapidly increasing PMF which initiates the next collapse. It is, of course, important that the state remain localized so that it maintains a significant PMF. Under some conditions for $D \geq 2$ a localized bound state can be lost, i.e., λ_0 crosses zero before sufficient PMF is built up to initiate collapse. For the D=3 scalar model discussed here we find a finite nucleation threshold [Rose et al.[19]]. For E_0 below this value the cycle cannot be maintained even for an isolated caviton.

These scalar model calculations have been used to deduce scaling laws[19,14] for the dependence of quantitites such as the electrostatic energy taken into collapse, the caviton cycle time and the maximum caviton radius as a function of driver strength E_0. We refer the reader to references 19 and 14 for details. As an example, we find that the peak electric field in the caviton collapse process scales as $|E|^2_{peak} \sim E_0^{-2}$; the peak field in the caviton decreases with increased driver strength. The caviton cycle period scales as $\tau \sim E_0^{-1}$ and the maximum caviton radius, $\Delta \sim E_0^{-1}$. From these we estimate the space-time density of cavitons to scale as $(\tau\Delta^3)^{-1} \sim E_0^4$.

This isolated collapse model is oversimplified in several ways, one is its neglect

of the turbulent environment of the collapse site. The density fluctuation n(r,t) was constrained so that there was locally no net change in particle number - i.e., $\int dr r^2 n(r,t)=0$ - i.e., the local averaged plasma frequency is the same as the global average plasma frequency which is the zero of frequency in our envelope approximation. This constrains all bound or localized states to have $\lambda_\nu(t)<0$. However, locally on a scale larger than a single caviton but macroscopically small there can be fluctuations in the background plasma frequency away from the global average. If the local plasma frequency is different from zero this is equivalent to replacing n(r,t) in (5.12a) by $\delta n_0 + n(r,t)$ and bound states can occur if $\lambda_\nu < \delta n_0$. Since there are local domains or "patches" of positive and negative δn_0 we conclude that in a large multicaviton system localized states can occur for $\lambda_\nu(t)<(\delta n_0)_{max}$ where $(\delta n_0)_{max} >0$ and depends on the parameters E_0, ω_0, etc. which determine the turbulent state. Simulations with $\omega_0 >0$ are consistent with this picture. The "localized" states for $\delta n_0 >0$ are not strictly localized from the mathematical point of view; their eigenfunctions may have extended tails which are exponentially small but do not decay at large distances. Such states are better described as resonance states as discussed at the end of this section.

The self similar scaling of the parameters of the eigenstates during the collapse phase are well-known [e.g., Galeev et al.[18]]. A self-similar ansatz for $\underline{e}_i(\underline{x},t)$ can be written

$$\underline{e}_i(\underline{x},t) = \frac{1}{\delta^{D/2}(t)}\,\hat{\underline{e}}(\underline{x}\delta^{-1}(t) \tag{3.18a}$$

where $\hat{e}(\zeta)$ is the normalized shape function of the collapsing state.

$$\int d\zeta|\hat{e}(\zeta)|^2 = 1 \tag{3.18b}$$

The collapses observed in our D = 2 simulations are not cylindrically symmetric as can be seen in Figure (4.2), but have a pancake shape with the narrow direction mainly aligned along the pump polarization (the x direction in Figure 1). The aspect ratio of the y dimension to the x dimensions appears to be in the range of 2 to 3. The ansatz of (3.18) implies that although the aspect ratio is not necessarily unity all dimensions scale with $\delta(t)$. Simulations of collapse in D = 3 for isolated

cavitons[22] and for multicaviton states[6] display these pancake cavitons whose orientation arises either as a result of initial conditions or by coupling to a drive source such as we have used.

The scaling of the parameters of the self-similar supersonic collapse depend on the spatial dimension D as follows:

$$\delta(t) = (t_c - t)^{2/D} \tag{3.19}$$

$$\lambda(t) \sim \delta^{-2}(t) \sim (t_c - t)^{-4/D} \tag{3.20}$$

where t_c is the time of collapse. The self-consistent density behaves as

$$n(\underline{x}, t) \;=\; -\frac{1}{\delta^2(t)}\, G(\underline{x}\delta^{-1}(t)) \tag{3.21}$$

where $G(\underline{x}\delta^{-1}(t))$ is a shape function related self-consistently to $\tilde{e}(\underline{x}\delta^{-1}(t))$. The scalar model collapse behavior is consistent with these scalings for D = 3.

We can sometimes use the self-similar formula (3.18) for $\underline{e}_i(\underline{x},t)$ in other regimes -- e.g., nucleation but where $\delta(t)$ does not satisfy the scaling of (3.19). Examples of the evolution of $\delta(t)$ in the scalar model are shown in Figure 3.

In the scalar model results, presented above, the contributions from nonlocalized states or from localized excited states are neglected. Such localized excited eigenfunctions have one or more nodes in the region of the confining density well and would be expected to couple less efficiently to the pump in the overlap integral of (5.9c). Localized excited states which evolve to collapse are not observed in the simulations.

For an isolated density well the localized state eigenfrequencies lie below those of the nonlocal (or continuum) states. In the "patchy" model with fluctuating domains of differing mean plasma frequency, it appears that the eigenvalue ranges of localized and nonlocalized states may overlap.

The definition of a localized state as one of the localized eigenfunctions $\underline{e}_i(\underline{x},t)$ is actually too restrictive. A wavepacket of nonlocalized states whose Λ_ν lie just above the localization limit can be a resonance state analogous to those known

in quantum mechanical scattering theory if it is a superposition of states with a sharp peak in the density of states. Such a resonance state will appear spatially coherent and localized for a time $\Delta t \sim (\Delta\lambda)^{-1}$ where $\Delta\lambda$ is the frequency width of the resonance. The resonance state will then have a ponderomotive force over a time which may be sufficiently long to depress the density so that a strictly localized eigenstate can again appear. The effective source terms $E_0 \bullet (e_\nu n)$ are nearly the same for all the states comprising the resonance. A narrow resonance state therefore cannot be distinguished from a strictly localized eigenstate and so the definition of the states $\underline{e}_i(x,t)$ which are identified in (3.11) should be extended to include such narrow resonance states. It can be shown that for a sufficiently narrow resonance the equation of motion for its amplitude $h_i(t)$ is indistinguishable from the equation of motion discussed above for a localized state. The existence of such resonances is another reason why localized states appear to exist for $\lambda_i > 0$. As discussed above, the random density environment of a caviton can also raise the eigenvalue limit for localization to positive values. Such localized states are also best described as resonance states.

4. POWER SPECTRA OF TURBULENT FLUCTUATIONS IN THE LOCAL CAVITON MODEL

It is well-known that the power spectrum of electron density fluctuation, $\tilde{n}_e(\underline{x},t)$, contains information concerning the elementary excitations of a plasma and can be measured by incoherent Thomson scatter techniques. For frequencies ω near the electron plasma frequency ω_p (or its negative) the ions cannot respond significantly and so one can relate the electron density fluctuation directly to the total electric field

$$4\pi e\, \tilde{n}_e(\underline{\tilde{x}},t) = \underline{\tilde{\nabla}} \cdot \underline{\tilde{E}}_{TOT}(\underline{\tilde{x}},t) \;=\; \frac{1}{2}\underline{\tilde{\nabla}} \cdot \underline{\tilde{E}}(\underline{\tilde{x}},t)e^{-i\omega_p t} \;+\; c.c. \qquad (4.1)$$

From this it is easy to see that the power spectrum of n_e is directly related to that of the envelope field. For $\tilde{\omega} \simeq \omega_p$ we have

$$\begin{aligned}(4\pi e)^2|\tilde{n}_e(\underline{\tilde{k}},\omega)|^2 &= (1/4)|\underline{\tilde{k}} \cdot\; \underline{\tilde{E}}(\underline{\tilde{k}},\tilde{\omega}-\omega_p)|^2 \\ &= (1/4)\lambda_D^2|\underline{\tilde{k}} \cdot \underline{\tilde{E}}(\underline{\tilde{k}},\tilde{\omega}-\omega_p)|^2(4\pi n_0 T_e)^{-1} \qquad (4.2)\end{aligned}$$

To obtain the low-frequency spectrum associated with the ion line we note that for $\tilde{\omega} << \omega_p$ that quasineutrality is obtained so $n_e(\tilde{\underline{k}}\ \tilde{\omega}) \simeq n_i(\tilde{\underline{k}},\tilde{\omega}) = n(\tilde{\underline{k}},\tilde{\omega})$ and the low frequency electron density spectrum is obtained directly from the density fluctuation which appears in the Zakharov model:

$$|\tilde{n}_e(\tilde{\underline{k}},\tilde{\omega}|^2 = |\tilde{\underline{n}}(\tilde{\underline{k}},\tilde{\omega})|^2 \tag{4.3}$$

The power spectra can be found by taking the temporal Fourier transform of (3.1).

$$\underline{E}(\underline{k},\omega)_T \ = \ \sum_i^{N(T)} \ expi[\underline{k}\cdot\ \underline{x}_i - \omega t_i]\underline{\varepsilon}_i(\underline{k},\omega)_t + \underline{E}(k,\omega)_{nonlocal} \tag{4.4a}$$

where

$$\underline{\varepsilon}_i(\underline{k},\omega)_t \ = \ \int_{t-T/2}^{t+T/2} dt(t'-t_i)\underline{\varepsilon}_i(\underline{k},t'-t_i)\ exp[i\omega(t'-t_i)] \tag{4.4b}$$

is the single event Fourier coefficient. If we make the assumption, that all events are uncorrelated we obtain the power spectrum as a sum over single event spectra:

$$\langle|\underline{E}(\underline{k},\omega)_t|^2\rangle \ = \ \sum_{i=1}^{N(T)} \ |\underline{\varepsilon}_i(\underline{k},\omega)|^2 \ \equiv \ N(T)\langle|\underline{\varepsilon}(\underline{k},\omega)|^2\rangle \tag{4.5}$$

The important effect of correlations will be discussed below.

Simulation parameters can be chosen so that the collapse events are so well separated in time that we were able to compute the single event spectra $|\underline{\varepsilon}\ (\underline{k},\omega)|^2$ for this case. These spectra, shown in Figure 5, have a surprisingly rich structure including the following features: 1.) Essentially all the spectra energy occurs for $\omega < \omega_0$; in this case $\omega_0 = 0$; 2.) There are well defined peaks in the spectrum; 3.) For increasing k, i.e., increasing $k\lambda_D$, the peaks for more negative ω become relatively more important; 4.) The position of the maximum shifts in a step-wise fashion (see inset to Figure 6) where $-\omega_{max} \sim$k, i.e., $\omega_p - \tilde{\omega}_{max} \sim \tilde{k}\ c_S$; 5.) There is a weak "free mode" peak at $\omega \sim k^2$, i.e., roughly at the Bohm-Gross frequency. These single event spectral properties are similar to those shown in Figure 6 for

the power spectra from multicaviton states in a magnetic field.[14] Caviton-caviton correlations also can have a strong effect on the spectral shape and will be discussed below.

We have obtained some insight into the sources of this structure from the scalar model discussed in Sec. 3. A realization of the single event spectrum $|\varepsilon\ (\underline{k},\omega)|^2$ for the scalar model is constructed by taking the temporal transform of the function $f(t) = h_0(t)e_0(k,t)$ for $0<t< \tau_c$ and $f(t) = 0$ for $\tau_c <t<T$ where T is chosen to give the desired frequency resolution and $e_0(k,t)$ is the spatial Fourier transform of the numerically obtained $e_0(r,t)$. The results are shown in Figure 7. These model spectra contain the features listed above for the D = 2 Zakharov model (Fig. 6) except for 4.) and 5.).

The predominance of negative frequencies arises because the phase velocity $\dot{\Phi}$ in Figure 4 is predominantly negative; this in turn is related to the negativity of the eigenvalue $\lambda(t)$. In this model calculation Eq. 3.7 reduces to $i\dot{h}_0 - \lambda_0 h_0 = S_0 \equiv E_0\langle e_0|n\rangle$ since we are neglecting coupling to excited states. Then if we write $h_0 = |h_0|\ \exp i\Phi_0$ we see that $\dot{\Phi}_0$ is related to λ_0 by

$$-\dot{\Phi}_0 = \lambda_0(t) + S_0(t)|h_0|^{-1}cos\Phi_0 \tag{4.6}$$

which is the equation used to compute Φ_0 in Figure 3.

The peaks arise from a modulation of the spectrum with an angular frequency $\Delta\omega = 2\pi/\tau_c$ where τ_c is the caviton lifetime as measured by the width in time of the total electrostatic energy pulse, $|h_0(t)|^2$, shown in Fig. (3). This is the same kind of modulation that arises in the spectrum of a single square wave pulse. Let us assume that the early-time spectrum from low-duty-cycle experiments can be identified with the incoherent average $\langle|\varepsilon(k,\omega)|^2\rangle$ of single-event spectra. In this averaged spectrum the individual spectral peaks may be smeared out but it is reasonable to assume that the half-power frequency width is approximately that of the first and strongest maximum of the single-event spectra. Application of this argument to the data of Djuth, Gonzales, and Ierkic[32] in this regime – e.g., their Figure 4 – leads also to a value $\tau_c \sim 0.1\pm0.05$ ms. The k dependence in this model arises from the k dependence of the eigenfunction, $e_0(k,t)$; for a localized state with $k\delta_0(t)$ we expect that $e_0(k,t)\sim \delta_0^{D/2}(t)\ \exp\ (-k\ \delta_0(t))$. For increasing k, smaller

values of $\delta_0(t)$ are favored and these correspond to more tightly collapsed states with more negative frequencies.

The free-mode peak observed in the spectra Figures 5 and 6 is, of course, not seen in this simplified scalar model calculation since it neglects all of the excited states. The free mode excitation in the scalar model is discussed below. The behavior near $\omega = 0$, including the shift of the maximum peak with k, is also different in the scalar model than in the D = 2 Zakharov simulation of Figure 5. The inclusion of excited states in the scalar model brings the results into closer qualitative agreement. In the case of overdense drive $\omega_0 < 0$, where free modes are only weakly excited, this single state model agrees well with the complete Zakharov simulations, such as those shown in Fig. 11.

The Fourier transform of E(r,t) is given by $E(k,\omega) \simeq \int dt \exp i\,(\omega t + \Phi_0(t))\,|h_0(t)|\,e_0(k,t)$ where Φ_0 is the phase of $h_0(t)$. For large negative ω we can make asymptotic estimates based on a stationary phase evaluation of the time integral; the stationary phase points $t = t_S$ occur approximately where $\omega = -\dot{\Phi}_0(t_S)$. From Fig. 2 we see that the ground state has large negative phase velocities where $\dot{\Phi}_0(t) \rightarrow -\lambda_0(t)$ as $t \rightarrow t_c$ and can satisfy the stationary phase condition. In this temporal regime one comes closest to the self-similar scaling for the collapsing state: $e_0(rt) = \delta_0(t)^{-D/2}\,\Psi_0(r/\delta_0(t))$ with the spatial Fourier transform $e_0(k,t) = \delta_0(t)^{D/2} \cdot \int d\xi\,(\exp - ik\delta_0\xi)\Psi_0(\xi)$. The self similar behavior is $\delta_0(t) \sim (t_c - t)^{2/D} \sim \lambda_0(t)^{-1/2}$ where t_c is the collapse time. Using these behaviors in the stationary phase evaluation of the Fourier integral we find the asymptotic behavior $|E(k,\omega)|^2 \sim |\omega|^{-(1+3D/4)}$ as $\omega \rightarrow -\infty$. This asymptotic prediction is observed in the D = 2 vector Zakharov simulations and in the scalar simulations to an accuracy of 10%.

The spectrum obtained from incoherent scatter of radars (ISR) from the modified ionosphere is the result of about 10^8 events and the question of caviton-caviton correlations becomes important. In general if the events are correlated, (4.5) is replaced by

$$\langle |\underline{E}(\underline{k},\omega)_t|^2 \rangle = \sum_i^N |\underline{\varepsilon}_i(\underline{k},\omega)|^2$$

$$+\sum_{i\neq j}^{N}\sum^{N} exp\ i[\underline{k}\cdot(\underline{x}_j-\underline{x}_i)-\omega(t_j-t_i)]$$

$$\cdot\ \underline{\varepsilon}_i(k,\omega)\cdot\underline{\varepsilon}_j^*(k,\omega) \tag{4.7}$$

The second or "coherent" term in this equation has N^2 potential contributions and so could have a potent effect on the spectrum if events are correlated.

A possible model of the effect of correlations is to assume that the dispersion in the single event transform $\underline{\varepsilon}_i(\underline{k},\omega)$ is small from event to event. This is true in the scalar model calculations and has been seen in the full vector simulation; especially in the case of overdense drive. Formally, this assumption is equivalent to writing $\underline{\varepsilon}_i(\mathrm{k},\omega) = \bar{\underline{\varepsilon}}(\underline{k},\omega) + \delta\underline{\varepsilon}_i(\underline{k},\omega)$ where $\bar{\underline{\varepsilon}}$ is the average over many events and $\delta\underline{\varepsilon}_i=0$. If we assume $|\delta\underline{\varepsilon}_i|^2 << |\bar{\underline{\varepsilon}}|^2$ we can write

$$\langle|\underline{E}(\underline{k},\omega)|_t^2 \simeq \langle|\rho(\underline{k},\omega)|^2\rangle|\bar{\underline{\varepsilon}}(\underline{k},\omega)|^2 \tag{4.8a}$$

where

$$\rho(\underline{k},\omega) \;=\; \sum_{i}^{N(T)} exp\ i[\omega\, t_i - \underline{k}\cdot\underline{x}_i] \tag{4.8b}$$

This quantity is just the space-time Fourier transform of the caviton event density

$$\rho(\underline{x},t) \;=\; \sum_{i}^{N(T)} \delta^D(\underline{x}-\underline{x}_i)\delta(t-t_i) \tag{4.9}$$

Eq. (4.8a) shows that in this approximation the single event spectrum $|\underline{\varepsilon}(\underline{k},\omega)|^2$ is modulated by the correlation or structure factor: $\langle|\rho\ (\underline{k},\omega)|^2\rangle$.

5. COMPARISON WITH OBSERVED POWER SPECTRA

Recently Cheung et al.[1] have performed modification experiments at Arecibo which emphasized low duty cycle heating sequences; the heater was turned on

periodically in pulses of duration up to 50 ms with an interpulse period (IPP) of 150 ms. The Thomson radar diagnostic pulses of duration 1.1 ms were also turned on and off with the same period and the delay time between the onset of the heater pulse and that of the radar pulse was varied. The comparisons between these observations and the SLT theory can be summarized as follows:

1.) For short radar delay times the many-pulse averaged observed spectra agree in detail with the smoothed simulation spectra. The main energy containing portion of these spectra occur for $\omega < 0$ and there is a free mode peak for $\omega > 0$.

Examples of experimental spectra from Cheung et al.[12] are shown in Figure 8. Examples of smoothed simulation spectra including geomagnetic field effects are shown in Figure 6 taken from DuBois et al.[14]

2.) The local caviton model accounts for the $\omega < 0$ spectral features as arising from the nucleation-collapse-burnout caviton cycle as discussed in Section 4.

3.) Associated with each caviton cycle a nearly free Langmuir wave packet is radiated away from each caviton site. This is discussed in Section 6. The free mode peak occurs at a frequency $\tilde{\omega}_f = \omega_p[1 + (3/2)(\tilde{k}\lambda_p)^2 + (1/2)\ (\tilde{\omega}_c/\omega_p)^2 \sin^2\theta]$ associated with a free Langmuir wave for which $\tilde{\omega}_f > \tilde{\omega}_H$ yet is a distinct signature of the collapse process.

4.) Recently Djuth[33] et al. have presented evidence that these short delay-time spectra are produced in a thin turbulent layer within 100 m of the reflection altitude of the heater. This is consistent with the parameters of our simulations for which we assumed the altitude of the first standing wave maximum of the heater in a smooth ionosphere density profile with a scale length of about 50 km. [This determines the value of $\tilde{\omega}_0 = \omega_H - \omega_p$.]

It is important to realize that these short delay time observations, following the onset of the heating pulse, are completely at odds with the predictions of weak turbulence theory (WTT). WTT fails to predict the spectral shape, the altitude dependence of the turbulence or its angular dependence (on the direction of $\underline{k}$ observed by the radar relative to the geomagnetic field.) SLT on the other hand accounts for all of these observations qualitatively and at least semi-quantitatively.

The observations of Djuth[33] et al. indicate that the turbulent layer begins to spread downward from the reflection altitude at about 50 ms, following the onset

of heating ultimately extending to an altitude 1 to 2 km below reflection after 100 ms or so. Changes in the spectrum occur on similar time scales.

In several sets of observations[34,31,32,12,33] sharp spectral peaks are observed to develop as the time delay of the radar pulse is increased following the onset of the heater pulse. In Figure 9, a 50-pulse average spectrum is shown in which the radar pulses occur 29 ms following the onset of a 30 ms heating pulse with a 150 ms IPP. This spectrum shows features observed in many previous long-time experiments[33] consisting of a main "decay line" peak lying about 3.0 ± 0.5 kHz below the heater frequency and two "cascade" peaks lying further below the heater frequency by 10.0 ± 0.5 kHz and 16.0 ± 0.5 kHz, respectively. This approximate "1:3:5" pattern of frequency displacements is sometimes associated with a weak turbulence cascade.[33]

6. CAVITON CORRELATIONS

The question to concern us next is whether such a spectral pattern can be explained in terms of caviton correlations? We have found that for overdense driving where $\tilde{\omega}_H < \omega_p$ (or $\omega_0 < 0$) stable cycles can be found with cavitons in ordered spatial arrays. In the case of overdense driving the turbulent state depends on initial conditions[14] or at least the memory of initial conditions decays more slowly in time than in cases where $\omega_0 > 0$.

We wish to present here an example of a correlated caviton state which has interesting properties and has led us to consider a class of perfectly correlated, alternating lattice models. This example is one of a class of simulations in which cavitons initially arranged in a regular array of sites persist at these sites, their cycles become very stable and become phase locked to one another in various temporal patterns.

In Figure 10 we show the initial locations of two density cavities which resulted from previous collapses and in which the initial electric field fluctuation is set to zero. This is the initial state for a simulation with $E_0 = 1.2$ and $\omega_0 = -25$ in scaled units. This value of ω_0 corresponds to a domain in physical units which is about 1% overdense. We note that for these parameters the system is stable to modulational instability but yet a energetic nonlinear state is sustained for long times because of these initial conditions. In Figure 11 we show the time series of the maximum value of $|E(x,t)|^2$ versus time as the system evolves into a periodic pattern. As time

increases each evolves into a strict limit cycle with period $\tau = 0.59$ with the cycles at the two sites becoming $\tau/2$ out of phase with one another.

In Figure 10 we also show the extended spatial periodicity implied by our periodic boundary conditions. This shows that the simulation is equivalent to two interpenetrating square lattices in which the • positions are all in phase but are $\tau/2$ out of phase with the + positions which themselves are all in phase. Examples of the computed spectra are shown in Figure 11 for $\theta = 0$ and $\theta = 45°$.

In Figure 11 the single event spectra, the $|\bar{\varepsilon}(\underline{k},\omega|^2$ in (4.8a), are also shown for the same values of (k,θ). These are easy to isolate from a single cycle at a given site. According to (4.8a) the single event spectrum modulates the spectrum of the structure factor. Comparison of the complete spectra and the single caviton spectra in Figure 11 verifies this.

In Figure 12 we show the ion line spectra obtained from the same simulations. Note, in the cases in which the plasma line spectra in Figure 12 has peaks at odd multiples of $2\pi/\tau$ (i.e. cases a and d) structure, the ion line consists of a symmetrical peak around $\omega = 0$ (corresponding to $\dot{\omega} = \omega_H$) and two displaced peaks at $\omega = \pm 2\pi/\tau$. These two displaced peaks are shifted by exactly the same frequency as the "decay line" peak in the plasma line spectra in Figure 11 a and d. This correlation of frequency shifts in the plasma line and ion line spectra has often been offered as evidence of the parametric decay instability; here we see that the same spectral correlation can arise from completely different physics!

These considerations lead us to postulate models in which the cavitons tend to order themselves in a regular three-dimensional lattice in overdense regions of the ionosphere. In the ionosphere application, because the heater field varies within the radar observed region, due to the antenna pattern and the altitude dependent Airy pattern, the spacing, a, of cavitons in the lattice varies on a scale large compared to a. In regions of most intense E_0, a will be smallest. The orientation of the lattice may also vary within the observed region. Our scalar model simulations show that for $E_0 \simeq 0.5$ V/m the maximum isolated caviton size is about 40 λ_D so we might expect an intercaviton spacing a > 80-100 λ_D or about 40-50 cm. At Arecibo the radar wavenumber is about 2π (35 cm)$^{-1}$ which means that low order Bragg scattering from such a lattice is possible with small adjustments of the lattice spacing which could arise through variations in E_0. We imagine that the observed region of the heated ionosphere contains domains of ordered cavitons whose lattice

spacing and orientation varies from domain to domain so that in some domain the Bragg resonance condition for the radar is satisfied. It is difficult to estimate how likely it is to have such a resonant domain present. These spatially and temporally ordered domains take some time to organize themselves after the onset of heating.

In the simplest interesting model the cavitons are arranged on two identical, interpenetrating lattices. In each lattice the cavitons undergo strict limit cycles with period τ but the cycles in the two lattices are displaced in time by $\tau/2$ as in the simulation of Fig. 10-12. The two lattices are symmetrically oriented with respect to each other in such a way that nearest-neighbor cavitons are members different lattices.

The structure factor $|\rho(\underline{k},\omega|^2$ for this model was analyzed in detail in Ref. 14. The structure factor as a function of $\underline{k}=2\ \underline{k}_{radar}$, the wavevector observed by the backscatter radar, has resonances when $\underline{k}$ is equal to certain discrete vector values, $\underline{K}_\nu$, known as reciprocal lattice vectors. These satisfy the condition $\exp(i\underline{K}_\nu\cdot\underline{x}_n)=1$ for all caviton locations, $\underline{x}_n$, in the lattice. The magnitude of these vectors is determined by the lattice spacing and structure and can be written as $|\underline{K}|_\nu = (2\pi/a)|A_\nu|$ where a is the smallest lattice spacing and the numbers $|A_\nu|$ are determined by the lattice symmetry. The resonance conditions, $\underline{k}=\underline{K}_\nu$, are called Bragg resonance conditions. The lowest order Bragg condition corresponds to the case where the lattice spacing a is equal to half the radar wavelength; $a=(1/2)\lambda$radar. In this case it was shown[14] that the frequency spectrum has peaks at $\omega=m(2\pi/\tau)$ where m is an odd, positive or negative, integer. The strength of these peaks is proportional to N_c^2 where N_c is the number of caviton events observed in the time interval of the radar pulse. Higher order Bragg resonances arise when a is a larger multiple of $(1/2)\lambda$radar. These more loosely packed lattices may have peaks at $\omega=m(2\pi/\tau)$ where m is either odd (as for the primary resonance) or even. Regions of higher E_0 will produce more tightly packed lattices. (Recall that the local caviton model results, summarized in Section 3, predicted that the maximum caviton radius scaled like E_0^{-1}.) We expect stronger radar signals from the regions of stronger E_0 with the primary Bragg resonance. In this case we have the 1:3:5 type spectrum with resonances at $\omega=m(2\pi/\tau)$, m = -1, -3, -5, and also with m=1, 3, 5 etc. Eq. (4.8) shows that the spectrum is the product of the structure factor, $|\rho(\underline{k},\omega)|^2$ and the single particle spectrum $|\varepsilon(k,\omega)|^2$.

The latter has most of its strength for $\omega < o$ ($\tilde{\omega} < \omega_H$) with only a small overlap of the rgion $\omega > o$, as in the examples in Fig. 11. Thus the complete spectrum, $|E(\underline{k},\omega)|^2$, has prominent peaks for m= -1, -3, -5—plus a weaker peak at m=+1. The latter can be identified with the often observed "anti-Stokes" line.

In Ref. 14 it was noted that because of the scalings $\tau \sim E_0^{-1}$ and $\Delta \sim E_0^{-1}$ that if we identify the caviton lattice spacing, a, with the maximum caviton radius, Δ, we have $\tau \sim a$. If the lattice domain is such as to satisfy the lowest Bragg resonance condition, $a = (1/2)\lambda radar = (\pi/k)$, we conclude that the downward frequency shift of the first decay line, $\Delta\omega = 2\pi/\tau \sim k$. This has the same k dependence as the ion acoustic frequency and is found, numerically, to be close to the ion acoustic frequency, within a factor of 2. This scaling of the frequency interval of the 1:3:5 spectrum is qualitatively the same as predicted by weak turbulence theory! It is remarkable that the correlated caviton model seems to be able to account for all the observed features of the radar power spectra.

However, there are two problems with this explanation. First, it is observed[35,36] that when the heater is switched off the spectral peaks of the 1:3:5 pattern remain for several ms after switch-off, albeit with decaying amplitudes and altered relative amplitudes. We can not see how the correlations necessary to preserve this spectral structure can be maintained in the correlated caviton model <u>after</u> switch-off of the heater. A second problem with the correlated caviton explanation are the recent observations of Djuth et al.[33] that the 1:3:5 structured spectra arise from turbulence excited 50-100 ms following heater turn on, at altitudes up to 1 to 2 km below the reflection altitudes. At such underdense altitudes, with respect to the undisturbed ionosphere, it is harder to imagine that ionospheric irregularities can produce the <u>overdense</u> domains necessary for correlations.

Our theoretical understanding, based mainly on simulation results and on a new microscopic theory of caviton correlations[37] <u>for the case of overdense driving</u>, can be summarized as follows:

i.) Temporal correlations at a given site devleop, on the time of a cycle period, into stable limit cycles.

ii.) Temporal correlations <u>between</u> sites evolve more quickly than spatial correlations between sites.

iii.) Some spatial patterns appear to be stable equilibrium arrangements with

definite temporal correlations between sites. Only temporal correlations where nearest-neighbor caviton cycles are in-phase or $\tau/2$ out of phase appear to be stable.

iv.) Those patterns which are not stable equilibria evolve to stable patterns on an experimentally relevant time scale - say tens of ms.

We have discussed (i) at some length above. An example of (ii) is the simulation discussed in relation to Figure 11 in which cavitons at neighboring sites became anti-correlated in time. Points (iii) and (iv) (as well as other examples of (i) and (ii) are based on simulations and theory which we will not present here. This work is part of our continuing research and will be published elsewhere.[37]

Near reflection altitude (critical density) it may not be difficult for ionospheric irregularities to produce the overdense domains necessary for correlations. If this is the case then why would the 1:3:5 spectral signature associated with caviton correlations <u>not</u> be observed? This could be due to a low probability of overdense domains which satisfy the spatial Bragg resonance condition for the particular radar wavelength.

Domains of coherent cavitons whose lattice spacing is not Bragg resonant for the given radar $\underline{k}$ are more likely to be present (near reflection altitude). Such domains will have weaker resonances at $\omega = 2\pi m\, \tau_d^{-1}$ for <u>all</u> m where the life time of the caviton cycle τ_d varies from domain to domain. The resonance at ω=0 is common to all domains and is not smeared out by domain to domain variations of τ_d as are the resonances for $m \neq 0$. The $\omega = 0$ resonance can be identified with what is conventionally called the "OTSI line" in ionospheric heating parlance. This line can be extremely narrow if the caviton cycles are long lived; we find $\Delta\omega \simeq \pi(M\tau_d)^{-1}$ where M is the number of cycles in the observation interval.[14] The caviton picture provides the only nonlinear description, which we know of, which is capable of understanding the very narrow width of the "OTSI line" observed in the experiments of Sulzer and Fejer.[38,39]

We believe, then, that it still remains a challenge to explain the 1:3:5 structured spectra which occur in some Arecibo observations 30-100 ms following the onset of heating. The results of Djuth et al.[33] show that the turbulence responsible for these spectral features occurs at significantly underdense altitudes with respect to the undisturbed ionosphere. We have carried out simulations[10] in such underdense regimes where $\omega_{ll} \quad \omega_p \simeq 3/2\ (k\lambda_l)^2\omega_p$. Again in such regimes caviton collapse

effects are strong: the dominant sink of Langmuir dissipation is through caviton collapse and the dominant sources of ion density fluctuations are the burnout density cavities remaining after collapse. We cannot expect WTT to describe such a turbulent state. On the other hand the fraction of Langmuir energy in free modes is significantly higher at these underdense altitudes than at reflection density or in overdense domains. We are investigating the possibility that the beating of the pump with the collapse-enhanced ion density fluctuations can produce a source for free Langmuir modes which would excite the decay (or Stokes) line and the weaker anti-Stokes line. (Similar processes may be possible for other steps in the "cascade.") The theory must take into account the direct excitation of free modes by collapse - (the $M_{\lambda\lambda_0}$ term in (7.4) which follows) - and the scattering of free Langmuir modes from collapse-enhanced ion density fluctuations. The latter process produces an effective damping on free Langmuir modes which tends to counteract the parametric gain which in WTT is supposed to lead to the usual WTT decay cascade. The results of this study will be published elsewhere.[40]

7. RADIATION OF FREE LANGMUIR WAVES BY COLLAPSING CAVITONS

Our studies have shown that the collapse process invariably excites free (or propagating) Langmuir waves. These manifest themselves in the "free mode" peak which occurs in all the power spectra, $|E(\underline{k},\omega)|^2$, which we have computed. As discussed in Sec. 5 there is strong evidence that the free mode peak has been observed in the short time scale experiments of Cheung et al.[12]

These free mode states are extended states whose energy is not localized at a particular point in space. A single collapsing caviton will radiate a wave packet of free modes which spread out and whose amplitudes decay geometrically (as r^{-1}) away from the excitation center of the caviton.

Outside of the spatial region of an isolated collapsing caviton these radiated Langmuir waves are asymptotically free Langmuir waves obeying the dispersion relation of (2.5). In a many-caviton environment, the large density fluctuations generated by collapse distort their propagation. The free mode frequencies appear to approach the dispersion relation (2.5) as k increases. For lower k values the frequencies are shifted to somewhat higher values due to the perturbation of the density fluctuations.

The generation of free modes can be understood in terms of the coupled mode amplitude equations (4.7). For simplicity we ignore the dissipative coupling (4.9b) which is not important for the k values measured by most radars. The coupling between states is given in (4.7) involving the matrix (4.9a)

$$M_{\nu\nu\prime} = i\langle \underline{e}_\nu \blacklozenge \dot{\underline{e}}_{\nu\prime} \rangle \tag{7.1}$$

By taking the time derivative of (3.2) and using the orthonormality condition (3.8) we can reexpress this as

$$M_{\nu\nu\prime} \;=\; i\,\frac{\langle \underline{e}_\nu | \dot{n} \blacklozenge \underline{e}_{\nu\prime} \rangle}{\lambda_\nu - \lambda_{\nu\prime}} \tag{7.2}$$

where

$$\langle \underline{e}_\nu | \dot{n} | \underline{e}_{\nu\prime} \rangle \;\equiv\; \int\, dx \underline{e}^*_\nu(xt) \bullet e_{\nu\prime}(xt)\, \frac{dn}{dt}\,(x,t) \tag{7.3}$$

The free modes have a continuum of eigenvalues $\lambda_\nu(t)$ in an infinite space and so we can parameterize them directly in terms of their eigenvalue λ;i.e., $\underline{e}_\lambda$ (x,t). The free modes receive from or give energy to localized states and are driven directly by the heater E_0. In the following we will consider in detail the coupling to a unique collapsing state denoted by the subscript zero. The equation of motion for the amplitude h_λ of a given free mode then follows from (4.7) as

$$i\,\dot{h}_\lambda + (\omega_0 - \lambda)h_\lambda + \int\, \rho(\lambda')M'_{\lambda\lambda\prime}h_{\lambda\prime} = -M_{\lambda\lambda_0}\,h_0 \;+\; E_0 \bullet \langle e_\lambda | n \rangle \tag{7.4}$$

Here

$$M_{\lambda\lambda_0} \;=\; i\,\frac{\langle \underline{e}_\lambda | \dot{n} | \underline{e}_{\lambda_0} \rangle}{\lambda - \lambda_0(t)} \tag{7.5}$$

and $\rho(\lambda')$ is the density of continuum states. The third term on the left hand side of (7.4) involving $M_{\lambda\lambda\prime}$ involves the scattering of one free mode from another. By considering the equation for

$$(d/dt)\,\sum_\lambda\, |h_\lambda(t)|^2$$

it is easy to see that the scattering terms do not change the total free mode energy while the terms on the right hand side of (7.4) do.

In Ref. 14 we have presented detailed numerical results for free mode radiation in the spherical scalar model discussed in Section 3. We found that, in the case of overdense driving, that the coupling to the time dependent collapsing Langmuir ground state, the $M_{\lambda\lambda o}h_o$ term in (7.4), dominates the dynamic conversion term, $E_0 <e_\lambda|n>$, in that equation. During the early nucleation stage of the caviton cycle, there is relatively little energy, $|h_o|^2$, in the local ground state and the dynamic conversion term is the dominant source of free mode energy. At intermediate times during collapse the coupling to the time dependent ground state is dominant and produces the largest free mode energies of the entire cycle. Deep into collapse the coupling to the ground state is again unimportant because the coupling coefficient, $M_{\lambda\lambda o}$, is going to zero as the coupling becomes more and more nonresonant. We also showed[14] that the hot electrons emitted during the burnout phase of collapse cannot produce a significant rate of production of free Langmuir waves by Cherenkov radiation.

As mentioned in Section 7, the energy in free modes is a higher fraction of the total Langmuir energy in the case of underdense driving ($\omega_H > \omega_p$). In the regime, $\omega_H - \omega_p > (3/2)(k\lambda_p)^2\omega_p$, the free modes occur at frequencies below the heater frequency, ω_H. The frequencies of localized states, which must be resonance states, apparently are in the range $\omega < \omega_H$ and overlap the free mode range. In these underdense regimes the emission and absorption of free modes by localized caviton states may be an important contribution to the nucleation process.[40]

In the experiments of Cheung et al.,[12] the ratio of the strength of the "collapse continuum" portion of the spectrum for $\omega < \omega_0$ to the strength of the free mode line increases as the time delay following the onset of the heating increases. It is observed that the strength of the free mode line does not change by as much as an order of magnitude while the strength of the collapse continuum increases by several orders of magnitude. This is consistent with the increase of the $\omega < \omega_0$ spectrum due to the onset of temporal correlations, i.e., a signal proportional to N_e^2 rather than N_e. The free mode line is not strengthened by correlations except in the unlikely case that the free mode peak at $\omega = \omega_f$ in the single caviton spectrum coincides with one of the correlation peaks at $\omega = 2\pi m/\tau_c$, which were discussed in Section 8. In addition, we know that free mode emission is weaker from overdense

regions where $\omega_0 < 0$ which are likely to be correlated. Note, for example, that the free mode peaks in the single caviton spectra from the correlated simulations of Figure 11 where $\omega_0 = -25$ are not very strong and do not produce prominent peaks in the correlated spectra.

8. CONCLUSIONS

We have discussed some of the accumulating evidence that strong Langmuir turbulence theory explains phenomena observed in laser-plasma interaction experiments and in ionospheric modification experiments. The laser-plasma experiments[10,11] particularly illuminate the sensitive coupling between low frequency density fluctuations and high frequency Langmuir fluctuations. The theory in refs. 13 and 29 appears to describe the major feature of the experiments of refs. 10 and 11 which are transient in nature. In these experiments a short pulse of SRS activity, as in Fig. 2, representing only one generation of collapse, is observed before the level of SBS ion sound fluctuations has grown sufficiently to detune the SRS process. In other experiments, say with longer laser pulses, under some conditions the SBS ion sound wave level may saturate at a level which permits a more or less continuous SRS excitation. A theoretical description of such a long time scale, SRS-excited, state of Langmuir turbulence is very difficult. Such studies are complicated by the need to apply realistic boundary conditions on the Langmuir waves and scattered light waves generated by SRS in an inhomogeneous density profiles. Numerical studies of such regimes have been carried out by Bonnaud et al.[41]

We have also explored in detail the implications of strong Langmuir turbulence theory for ionospheric heating experiments. The short time scale data from these experiments provide the best test of the theory available today. A major conclusion of our work is that weak turbulence theory (WTT) cannot be valid for the conditions of ionospheric heating. Our conclusion is based, first of all, on extensive numerical solutions of Zakharov's model encompassing many generations of collapsing cavitons. WTT follows under very special conditions from the Zakharov equations. The fact that the numerical solutions are dominated by coherent, collapsing cavitons proves that the nonlinear state is far from the regime of WTT. Recently Payne, Nicholson and Shen[28] have explored in detail the limit of WTT in numerical solutions of Zakharov's equations in one dimension and have established

rough criteria for the validity of WTT. These stringent criteria are not satisfied for the conditions of ionospheric heating.

The strong Langmuir turbulence theory has developed on two levels. The first level is based on solutions of Zakharov's model equations. From the properties of these solutions we have proposed the local caviton model which is a more "phenomenological" level. The local caviton model is built on single caviton properties. Cavitons go through cycles of nucleation, collapse and burnout. Associated single caviton properties include their lifetimes (or cycle times) τ_c, the single caviton field fluctuation $\underline{\varepsilon}(\underline{x},t)$ and its power spectrum $|\underline{\varepsilon}(k,\omega)|^2$. These single caviton properties are not necessarily those of isolated cavitons, although the isolated caviton approximation is at least qualitatively useful in many cases. As the driving becomes increasingly overdense ($\omega_0 < 0$) we have evidence that caviton interactions decrease but the residual interactions can lead to coherent caviton states. It is a challenge to understand the mechanism(s) for self-organization of this weakly interacting caviton gas. For these highly correlated states, the name turbulence hardly seems appropriate.

We believe that the <u>qualitative</u> properties of the local caviton model will be those deduced from the Zakharov model. More complete and accurate descriptions of single caviton properties are needed to treat the end stages of collapse and the burnout processes, whereas the nucleation and early collapse stages should be accurately described by the model. We anticipate that these improvements will make quantitative but not qualitative changes in the picture developed in this paper.

We believe that the SLT model has at least three apparent successes in explaining the ionospheric heating observations for early times (<50 ms) following the onset of the heating pulse:

1.) The altitude dependence of the early time plasma line signal is easily explained because the localized caviton states are <u>not</u> tied to the linear dispersion relation, (2.5). Based on the sensitive dependence of the turbulence level on E_0 we concluded[14] that the strongest plasma line signal should occur near the altitude of strongest E_0, which is the first Airy maximum in an undisturbed profile. This is in agreement with the early time observations of Djuth et al.[33]

2.) At these early times following the onset of heating the broad featureless spectrum for $\tilde{\omega} < \tilde{\omega}_{II}$, observed in many experiments,[12,31,32,33] is explained by

the dynamics of local caviton states. This part of the spectrum arises from the caviton cycle of nucleation-collapse-burnout. It is not consistent with WTT.

3.) A new prediction of SLT theory, the free mode peak, has been unambiguously observed by Cheung et al.[12] This arises because of the radiation of free Langmuir waves by collapsing cavitons. Again this feature is not consistent with WTT.

There is no experimental evidence concerning the dependence of this early time turbulence on the angle θ between the radar $\underline{k}$ and the geomagnetic field. The theory predicts that the same qualitative features would be seen at Tromsø where $\theta \sim 0°$ as observed at Arecibo where $\theta \sim 45°$, but the plasma line signal should be several orders of magnitude stronger at $\theta \sim 0°$. Short time scale experiments have not been carried out at Tromsø.

The SLT theory appears to be able to predict, at least qualitatively, many properties of the sharp spectral features observed at longer delay times following the onset of heating. These predictions depend on the existence of overdense domains of temporally and spatially correlated cavitons. Structures similar to the "decay line," the 3:5:7--"cascade lines" and the anti-Stokes line appear in the SLT spectrum of correlated cavitons provided Bragg resonance conditions, depending on the radar wavelength, are satisfied by some correlated domains. In addition we have new theoretical insight into the caviton-caviton interaction mechanisms which establish these correlations.[37] However, inspite of the attractiveness of this scenario, we believe this is probably not the mechanism which produces the above mentioned sharp spectral features. The reasons for this conclusion were given in Section 6.

The probability of finding Bragg resonant domains in the observed region may be small. However, there may be overdense domains of correlated cavitons, near reflection altitude, whose long-lived temporal correlations produce the narrow "OTSI" lines observed by Sulzer and Fejer.[38,39] We know of no other satisfactory explanation of such lines which takes into account the nonlinear evolution of the OTSI instability. Single pulse radar taken by Cheung et al.[12] and more recently by Sulzer et al.[12] may be consistent with temporal correlations at relatively early times following the onset of heating.

An alternative SLT scenario which might account for the sharp spectral features at later delay times was mentioned in Section 6. This theory must be consistent with

the new information from Djuth et al.[33] concerning the altitude of the turbulence producing these features. The theory must also be consistent with our observations that simulations of Zakharov's equations[40] for these underdense altidues show that a significant source of Langmuir dissipation and of ion density fluctuations is caviton collapse. Clearly WTT does not satisfy these requirements.

These questions are a challenge for future work. We believe that the new strong Langmuir turbulence model presented here is considerably more successful in describing the early-time behavior of the heated ionosphere than the conventional theory. We hope this paper will stimulate new experimental and theoretical tests of these ideas.

ACKNOWLEDGMENTS

We are grateful to Drs. P. Y. Cheung, T. Tanikawa, J. Santoru and A. Y. Wong for important collaborations and discussion. We are also grateful to Dr. F. T. Djuth and Dr. M. P. Sulger for permission to discuss their unpublished experimental results. Continuuing discussions and collaborations with Bandel Bezzerides are gratefully acknowledged. This research was supported in part by the U.S. Department of Energy, the Office of Naval Research, the Los Alamos Center for Nonlinear Studies and the Institute for Geophysics and Planetary Physics.

REFERENCES

1. D. F. DuBois and M. V. Goldman, Radiation induced instability of electron plasma oscillations, Phys. Rev. Lett. **14**, 544, 1965. V. P. Silin, Parametric Resonance in a plasma, Soc. Phys. JETP, Engl. Tranl. **21**, 1127, 1965.

2. M. V. Goldman and D. F. DuBois, Stimulated Scattering of Light from Plasmas, Physics of Fluids, **8**, 1966.

3. V. E. Zakharov, Collapse of Langmuir waves, Sov. Phys. JETP, 35, 908, 1972.

4. D. Russell, D. F. DuBois and H. A. Rose, Nucleation in Two-Dimensional Langmuir Turbulence, Phys. Rev. Lett. **60**, 581-584.

5. D. F. DuBois, Harvey A. Rose and David Russell, Power spectra of fluctuations in strong Langmuir turbulence, Phys. Rev. Lett. **61**, 2209, 1988.

6. P. A. Robinson, D. L. Newman and M. V. Goldman, Three dimensional strong Langmuir turbulence and wave collapse, Phys. Rev. Lett. **61**, 702, 1988.

7. G. D. Doolen, D. F. DuBois and H. A. Rose, Nucleation of cavitons in strong Langmuir turbulence, Phys. Rev. Lett. **54**, 804-807, 1985.

8. D. Russell, D. F. DuBois and H. A. Rose, Collapsing caviton turbulence in one dimension, Phys. Rev. Lett. **56**, 838-842, 1986.

9. P. Y. Cheung and A. Y. Wong, Three dimensional self-collapse of Langmuir waves Phys. Rev. Lett. **52**, 1222 (1984).

10. C. J. Walsh, D. M. villeneuve, and M. A. Baldis, Electron Plasma-Wave Production by Stimulated Raman Scattering: Competition with Stimulated Brillouin Scattering, Phys. Rev. Lett. **53**, 1445 (1984).

11. D. M. Villeneuve, H. A. Baldis, and J. E. Bernard, Suppression and Stimulated Raman Scattering by Seeding of Stimulated Brillouin Scattering in a Laser-Produced Plasma, Phys. Rev. Lett. **59**, 2547 (1987).

12. P. Y. Cheung, A. Y. Wong, T. Tanikawa, J. Santoru, D. F. DuBois, Harvey A. Rose, and David Russell, Short time scale evidence for strong Langmuir turbulence in H-F heating of the ionosphere, Phys. Rev. Letters **62**, 2676 (1989).

13. H. A. Rose, D. F. DuBois and B. Bezzerides, Nonlinear Coupling of Stimulated Raman and Brillouin Scattering in Laser-Plasma Interactions, Phys. Rev. Lett. **58**, 2547-2550, 1987.

14. D. F. DuBois, H. A. Rose and David Russell, Excitation of Strong Langmuir Turbulence Near Critical Density; Application to HF Heating of the Ionosphere, Los Alamos National Laboratory Report LA-UR-89-1419 submitted to Journal of Geophysical Research.

15. A. A. Vedenov and L. I. Rudakov, Interactions of waves in continuous media, Sov. Phys. Dokl. **9**, 1073 (1965).

16. K. Nishikawa, Parametric excitation of coupled waves. I. General formulation, J. Phys. Soc. Japan, 24, 916-922, 1968a, and Parametric excitation of coupled

waves. II. Parametric plasma-photon interactions, J. Phys. Soc, Jap. 24, 1152-1158, 1968b.

17. H. A. Rose and M. I. Weinstein, On the bound states of the nonlinear Schrödinger equation with a linear potential, Physica D, 30, 207-218, 1988a.

18. A. A. Galeev, R. Z. Sagdeev, Yu S. Sigov, V. D. Shapiro, and V. I. Schevchenko, Nonlinear theory for the modulational instability of plasma waves, Fiz. Plazmy 1, p 10, 1975 [Sov. J. Plasma Phys. 1 p 5, 1975].

19. H. A. Rose, D. F. DuBois, David Russell, and B. Bezzerides, Experimental signatures of localization in Langmuir wave turbulence, Physica D 1988b.

20. J. C. Weatherall, J. P. Sheerin, D. R. Nicholson, G. L. Payne, M. V. Goldman, and P. J. Hansen, Solitons and ionospheric heating, J. Geophys. Res. 87, 823-832, 1982.

21. V. E. Zakharov and L. N. Shur, Self similar regimes of wave collapse, Sov. Phys. JETP **54**, 1064, 1981.

22. A. I. Dyachenko, V. E. Zakharov, A. M. Rubenchik, R. Z. Sagdeev and V. F. Shvets, Two dimensional Langmuir collapse and two dimensional Langmuir cavitons, Pis'ma v ZhETF **44**, 504 (1986) [JETP Letters, 44, 648, 1986].

23. A. I. Dyachenko, A. M. Rubenchik, R. Z. Sagdeev, V. F. Shvets, and V. E. Zakharov, Computer simulation of the Langmuir collapse of the isolated cavity in Plasma Theory and Nonlinear and Turbulent Processes in Physics, Vol. 2, ed. by V. G. Bar'yakhtar et al., World Scientific 1987.

24. C. Aldrich, B. Bezzerides, D. F. DuBois and H. A. Rose [1984 unpublished].

25. V. E. Zakharov, A. N. Pushkarev, A. M. Rubenchik, R. Z. Sagdeev and V. F. Shvets, Final stage of 3D Langmuir collapse, JETP Lett. **45**, #8, 287 (1988) [Pis'ma Zh. Eksp. Teor. Fiz. **47**, #5, 239 (1988)].

26. B. D. Fried, and R. W. Gould, Longitudinal ion oscillations in a hot plasma, Phys. Fluids 4, 139 (1961).

27. D. R. Nicholson, Plasma Theory, John Wiley & Sons, N.Y., 1983.

28. G. L. Payne, D. R. Nicholson, and M. M. Shen, Numerical test of weak turbulence theory, to be published in Physics of Fluids.

29. A. Y. Wong and P. V. Cheung, Three dimensional self-collapse of Langmuir waves, Phys. Rev. Lett. **52**, 1222, 1984.

30. H. A. Baldis, P. E. Young, R. P. Drake, W. L. Kruer, Kent Estabrook, E. A. Williams, and T. W. Johnston, Competition between the stimulated Raman and Brillouin scattering instabilities in 0.35-μm irradiated CM foil targets, Phys. Rev. Lett. **62**, 2829 (1989).

31. A. Y. Wong, G. J. Morales, D. Eggleston, J. Santoru, and R. Behnke, Rapid conversion of electromagnetic waves to electrostatic waves in the ionosphere, Phys. Rev. Lett. **47**, 1340, 1981.

32. F. T. Djuth, C. A. Gonzales and H. M. Ierkic, Temporal evolution of the H-F-enhanced plasma line in the Arecibo F region, J. Geophys. Res. 91, p 12,089-12,107, 1986.

33. F. T. Djuth (private communication).

34. J. A. Fejer, C. A. Gonzales, H. M. Ierkic, M. P. Sulzer, C. A. Tepley, L. M. Duncan, F. T. Djuth, S. Gangulys, and W. E. Gordon, Ionospheric modification experiments with the Arecobø Heating Facility, J. Atmos. Terr. Phys. 47, p. 1165, 1985.

35. A. Y. Wong, Nonlinear Phenomena in laboratory and space plasmas, Physica Scripta T2/1, 262-270, 1982.

36. P. Y. Cheung (private communication).

37. Harvey A. Rose, D. F. DuBois and David Russell (to be published).

38. M. P. Sulzer, H. M. Ierkic, J. A. Fejer and R. L. Showen, HF-induced ion and plasma line spectra with two pumps, J. Geophys. Res., **89**, 6804, 1984.

39. M. P. Sulzer, H. M. Ierkic, and J. A. Fejer, Observational limitations on the role of Langmuir cavitons in ionospheric modification experiments at Arecibo, J. Geophys. Res. (1988).

40. D. F. DuBois, David Russell and Harvey Rose (to be published).

41.

42. M. P. Sulzer (private communication).

Figure captions.

Fig. 1. Two-dimensional plots of $|E|^2$ (upper surface) and n (lower surface) at two different times. Parameters in scaled units $E_0 = 1.2$, $\nu_i = 0.9$, $\omega_c/\omega_p = 0$, ν_e = Landau damping continued smoothly as k^2 at large k, $m_i/\eta m_e = 1836$, $L_x = L_y = 2\pi$ and a 128 × 128 spatial grid. The collapses are anistropic with the narrow dimension along the x axis, the drive direction.

Fig. 2. (a),(b) Spatial profiles of $|E|^2$, n and $|A_R|^2$ for two times for $n_o/n_c = 0.045$, L = 15 λ_o and $V_{osc}|c = 0.035$. Here E, n and A_R are, respectively, the Langmuir field envelope, the ion density fluctuation and the envelope of backscattered light wave; n_o is the electron density in the simulation slab of length L and n_c is the critical (reflection) density of the light which is incident on the slab from the left and has an intensity expressed in terms of the oscillating velocity V_{osc} - $(e/m\omega_o)E_{light}$. The units are $4\pi n_o T_e/439$ for $|E|^2$, $n_o/2754$ for n, arbitiary units for $|A_R|^2$, 91 λ_{De} is the spatial unit, and 140 psec is the temporal unit. We show only the leftmost portion of the slab, $0 \leq x \leq 3\lambda_o$. (c) Temporal history of the total Langmuir energy, total ion wave energy, and SBS backscatter reflection coefficient (in arbitiary units) for the case above. The unit of time is 150 ps. (d) Same but for $V_{osc}/c = 0.07$, $n_o/n_c = 0.055$. Here the unit of time is 132 ps. The mean square thermal fluctuations of the initial undisturbed plasma were $\langle|E|^2\rangle_{thermal} \simeq 0.1$ and $\langle n^2\rangle_{thermal} \sim 900$. In (c) and (d) note the initial pulse of Langmuir energy associated with a single generation of collapse and burnout followed by the growth of SBS backscattered light.

Fig. 3. The temporal evolution of (a) $|E(r = 0,t)|^2$ and n(r = 0,t), (b) $\lambda_0(t)$ and the phase velocity $-d\Phi/dt$ and (c) the caviton width $\delta(t)$ and the electrostatic energy in the caviton $|h_0(t)|^2$ in the scalar model; $E_0 = 1.8$, $m_i/\eta m_e = 2 \times 10^4$, $\nu_i = 0.9$ and $\omega_0 = 0$.

Fig. 4. Scalar model for $E_0 = 1.8$, $m_i/\eta m_e = 2\times10^4$, $\nu_i = 0.9$, $\omega_0 = -80$. Showing shape of n(r,t) and $|E(r,t)|^2$ as functions of r for two times in the caviton cycle evolution and the profiles of the two lowest eigenfunctions $e_0(r,t)$ and $e_1(r,t)$ vs r at the same times. The qualitative behavior is the same for the case ω_0 0.

Fig. 5. Spectra, $|\Psi(k,\omega)^2 = k^{-4}|\underline{E}(\underline{k},\omega|^2$, for D = 2 isolated collapse events. E_0 0.8, ν_i 0.9, $m_i/\eta m_e = 1836$, $\omega_0 = 0$. $k_x = 8$, $k_y = 0$. Inset Solid line, nega

tive frequency at maximum of spectrum vs $k = k_x$; dashed line, ion acoustic frequency shift, $|\omega| = k$.

Fig. 6. Power spectra $|E(\underline{k},\omega)|^2$ $E_0 = 1.2$, $\omega_0 = 5$, $\omega_c/\omega_p = 0.2$, $L_x = L_y = 2\pi$, M = 1836. Spectra are smoothed over an angular frequency interval $\Delta\omega \simeq \pi$. Spectra intensity scales are arbitrary. The spectra are for various values of (k,θ). Because of a numerical coincidence, when these results are scaled to the more realistic value $M = 9 \times 1836$, the frequency scales can also be read as kHz of frequency (not angular frequency).

Fig. 7. Power spectra $|E(\underline{k},\omega)|^2$ for the scalar model parameters of Fig. 2. Spectrum for $k = 40.0$.

Fig. 8. Experimental spectra. (a) Heater pulse width 10 ms, Interpulse period (IPP) 150 ms, $f_H = 7.3$ MHz spectra taken in 1.1 ms internals delayed 4 ms from onset of heating pulse. Note the free mode peak at ~ 72 kHZ above the heater frequency which is 256 on the scale, (b) Heater pulse width 10 ms, IPP 150 ms, $f_H = 7.3$ MHz spectral delayed by 1.5 ms from onset of heating. Free mode peak at 52 kHz. From Cheung et al. [1989].

Fig. 9. Plasma line spectra for 30 ms, heater pulses with 150 IPP at 7.3 Mhz and radar pulse delayed by 29 ms after onset of heater pulse, averages over 10 and 50 radar pulses, respectively.

Fig. 10. Two dimension simulation of alternating lattice model. Caviton locations marked • are $\tau/2$ out of phase with locations marked +. The caviton cycle period is τ. The central square is the simulation cell. The other cells are implied by the periodic boundary conditions. The •'s and +'s denote the initial caviton locations which do not change for $\omega_0 = -25$ or $\omega_0 = -15$. Other parameters: $E_0 = 1.$, $v_i = 0.9$, $m_i/\eta m_e = 1846$.

Fig. 11. Total correlated power spectra $|E(k,\omega)|^2$ (sharp line spectra) and single caviton spectra $|\varepsilon(k,\omega)|^2$ (smooth spectra) for the coherent alternating lattice for various values of (k,θ). Showing spectra for even and odd values of $n = (1/2\pi)$ $k \cdot$ where $\underline{d}$ is the displacement vector between the • and + lattices (see ref. 14) d. Here $|\mathcal{E}(\underline{k},\omega)|^2 = k^{-4}|E(k,\omega)|^2$ or $k^{-4}|\varepsilon(k,\omega)|^2$ for the two classes of spectra, respectively.

Fig. 12. Ion line spectra $|n(\underline{k},\omega)|^2$ for the coherent alternating lattice simulation. Both the total spectrum and the single caviton spectrum are again shown.

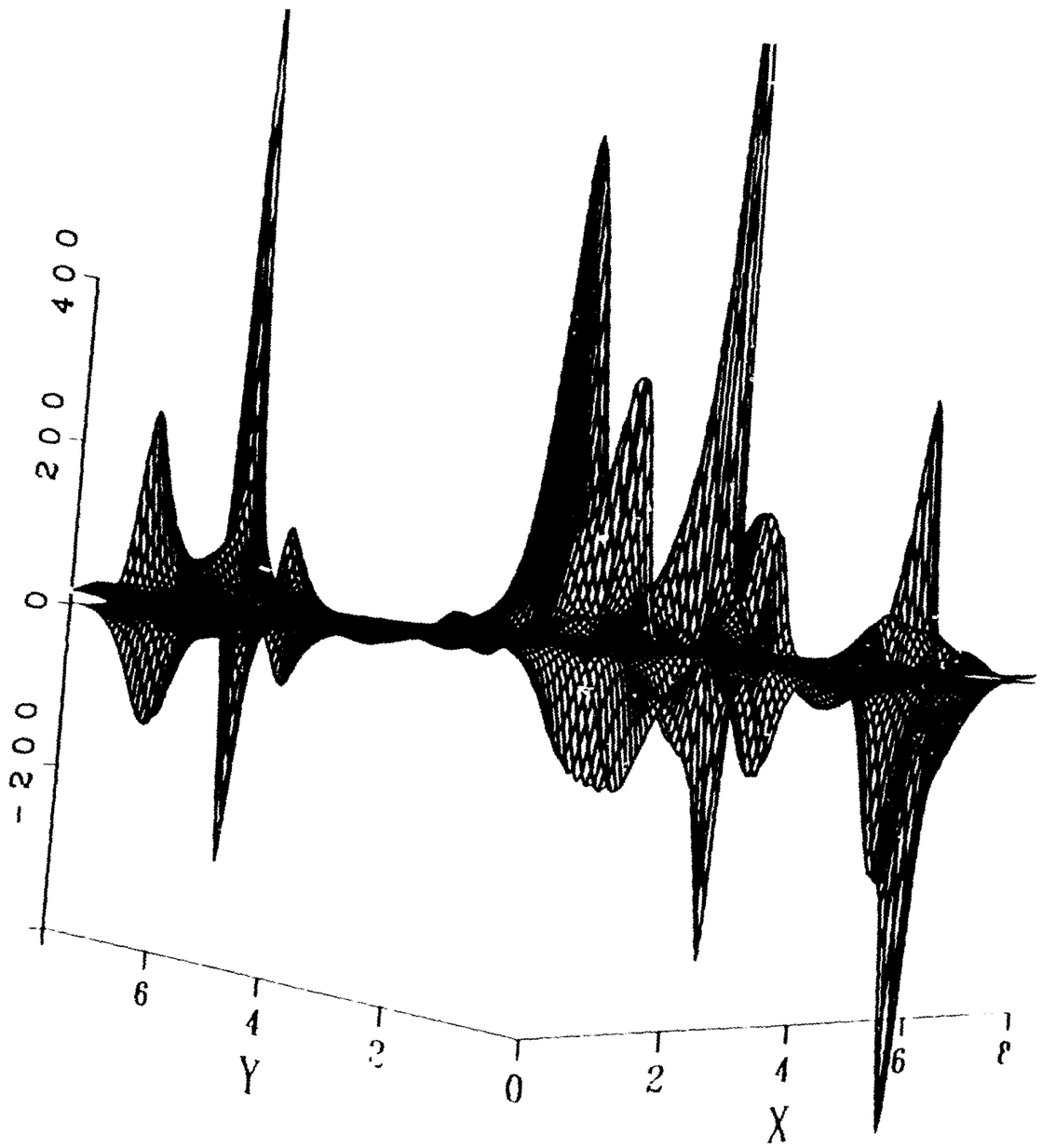
400
200
0
-200
6
4
2
Y
0
2
4
6
X

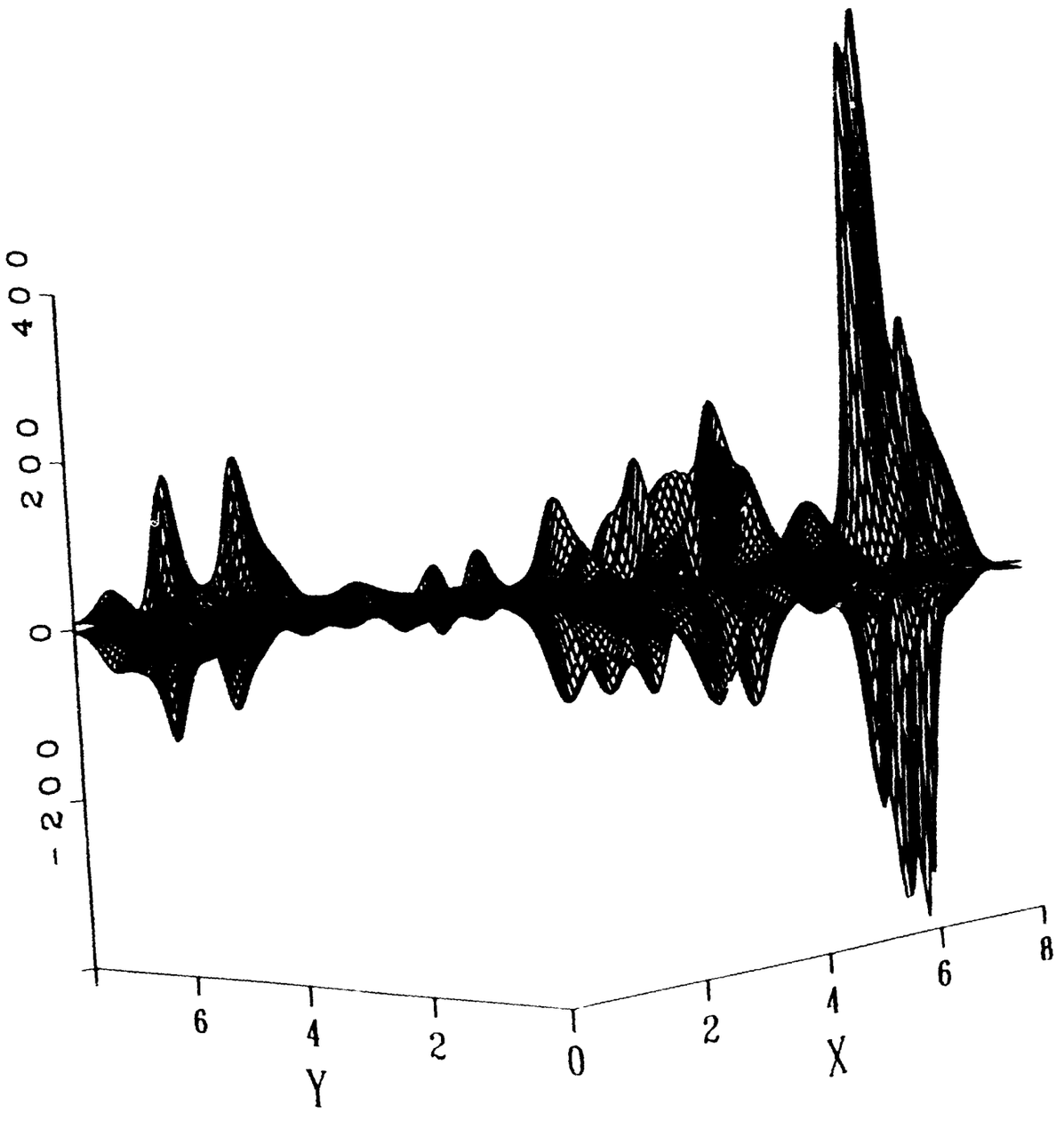
400
200
0
-200
6
4
2
0
Y
0
2
4
6
8
X

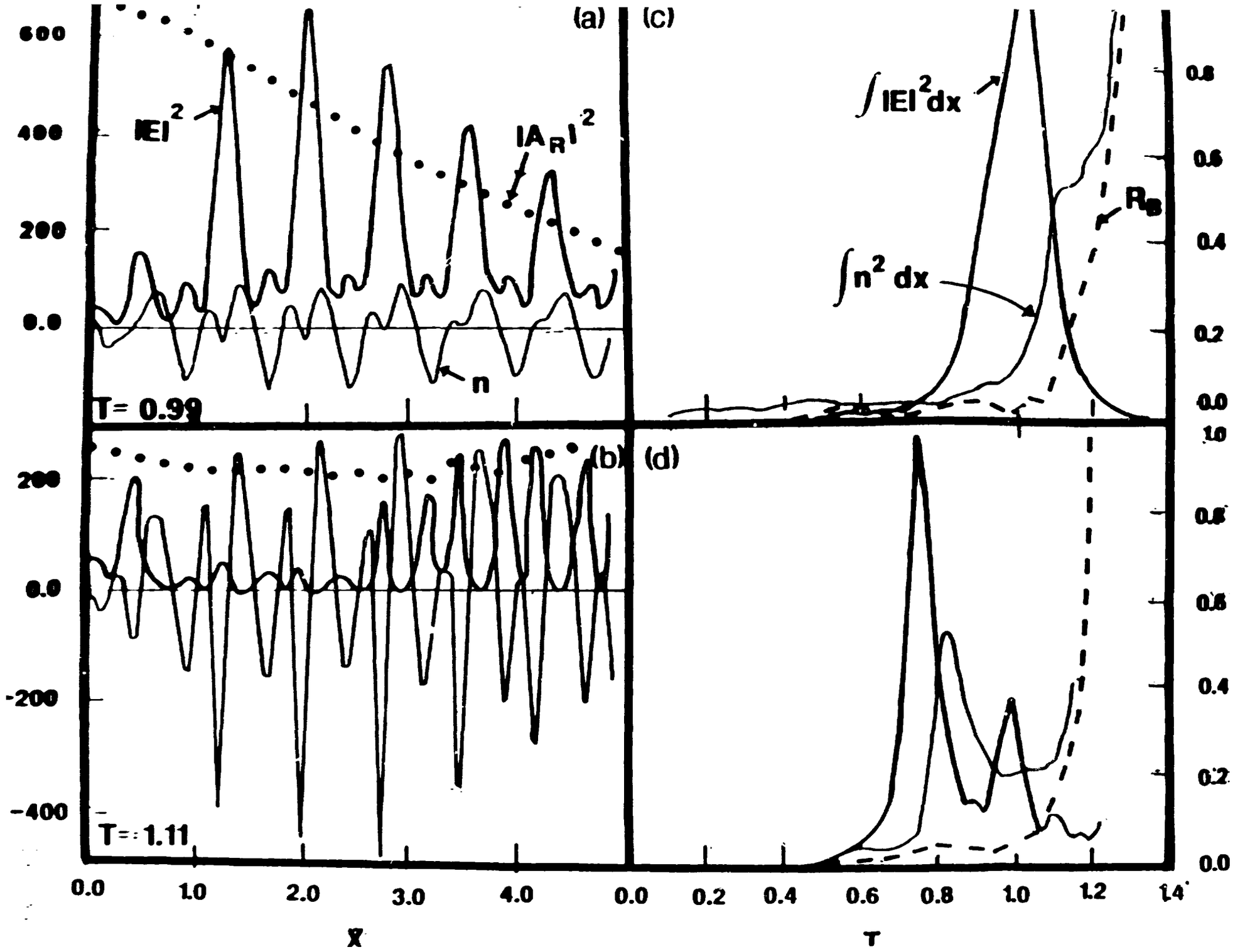
(a)
(b)
(c)
(d)
$|E|^2$
$|A_R|^2$
n
T= 0.99
T= 1.11
$\int |E|^2 dx$
$\int n^2 dx$
R_B
600
400
200
0.0
-200
-400
0.8
0.6
0.4
0.2
0.0
1.0
0.0
1.0
2.0
3.0
4.0
0.2
0.4
0.6
0.8
1.2
1.4
X
T

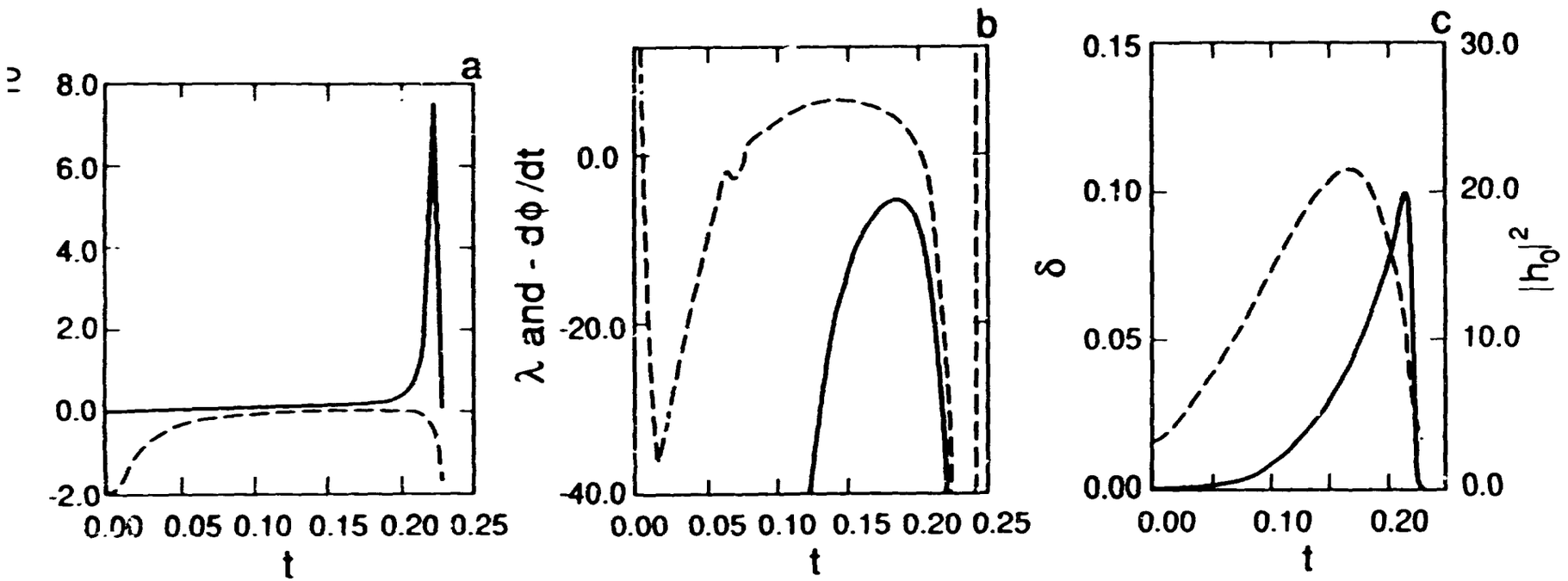
a
8.0
6.0
4.0
2.0
0.0
-2.0
0.00 0.05 0.10 0.15 0.20 0.25
t
b
λ and - dϕ/dt
0.0
-20.0
-40.0
0.00 0.05 0.10 0.15 0.20 0.25
t
c
δ
0.15
0.10
0.05
0.00
30.0
20.0
10.0
0.0
$|h_0|^2$
0.00 0.10 0.20
t

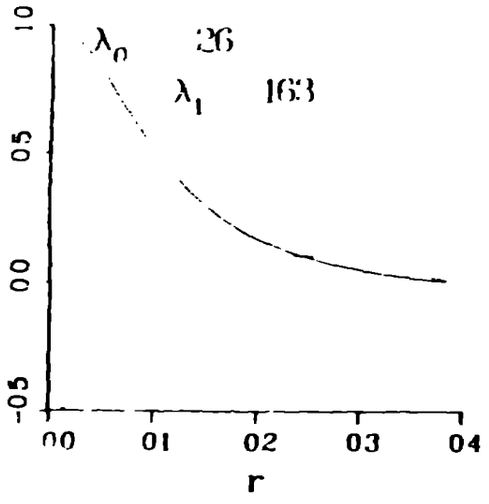
λ_0 26
λ_1 163
1.0
0.5
0.0
-0.5
0.0
0.1
0.2
0.3
0.4
r

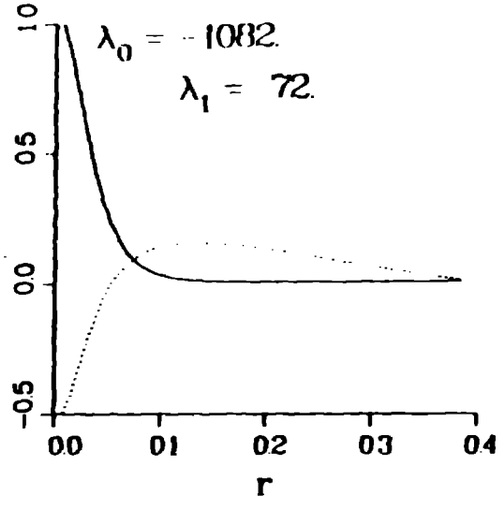
λ_0 = -1082.
λ_1 = 72.
1.0
0.5
0.0
-0.5
0.0
0.1
0.2
0.3
0.4
r

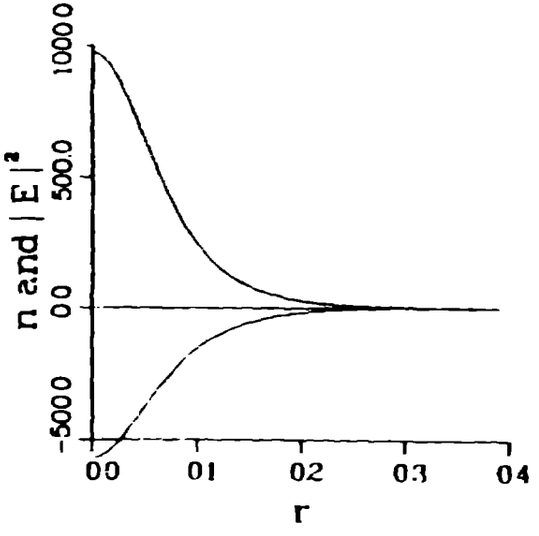
n and | E |²
10000.0
5000.0
0.0
-5000.0
0.0
0.1
0.2
0.3
0.4
r

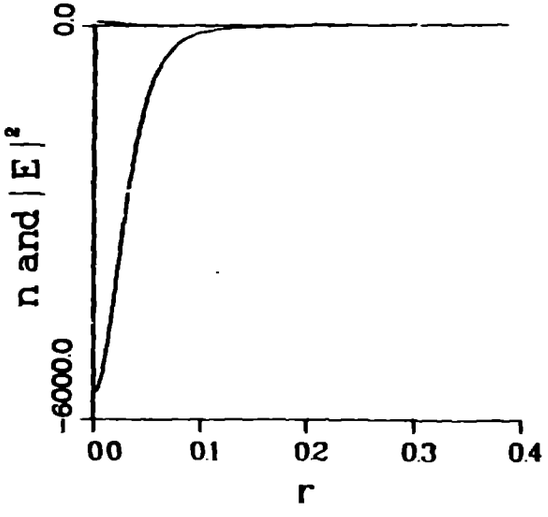
n and | E |²
0.0
-6000.0
0.0
0.1
0.2
0.3
0.4
r

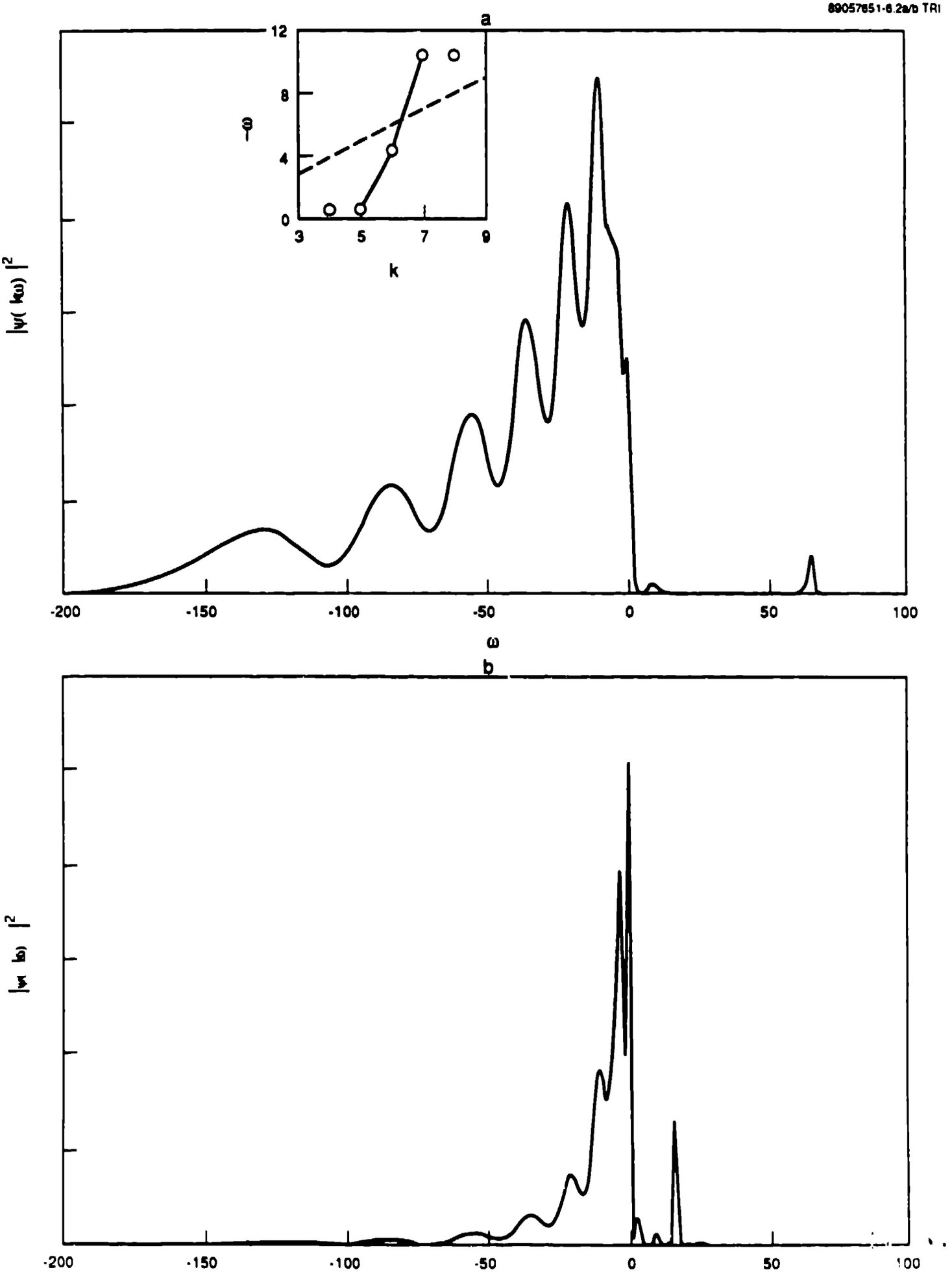
a
12
8
4
0
3
5
7
9
k
$|\psi(k\omega)|^2$
-200
-150
-100
-50
0
50
100
ω
b
$|\psi(k\omega)|^2$
-200
-150
-100
-50
0
50
100

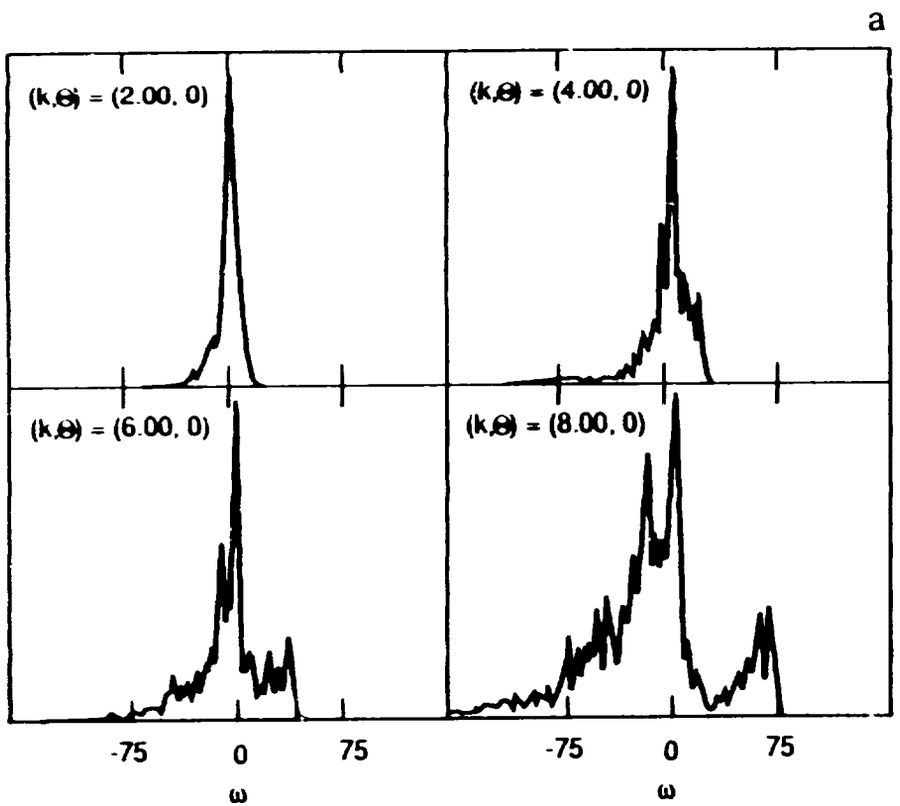
a
(k,Θ) = (2.00, 0)
(k,Θ) = (4.00, 0)
(k,Θ) = (6.00, 0)
(k,Θ) = (8.00, 0)
-75
0
75
ω
-75
0
75
ω

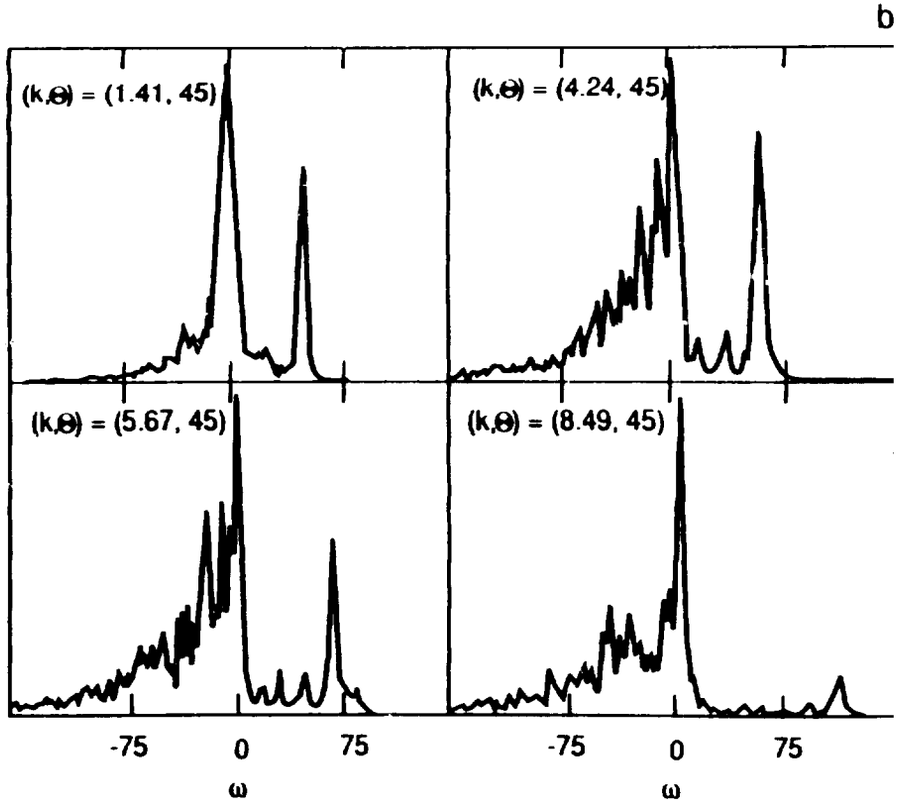
b
(k,Θ) = (1.41, 45)
(k,Θ) = (4.24, 45)
(k,Θ) = (5.67, 45)
(k,Θ) = (8.49, 45)
-75
0
75
ω
-75
0
75
ω

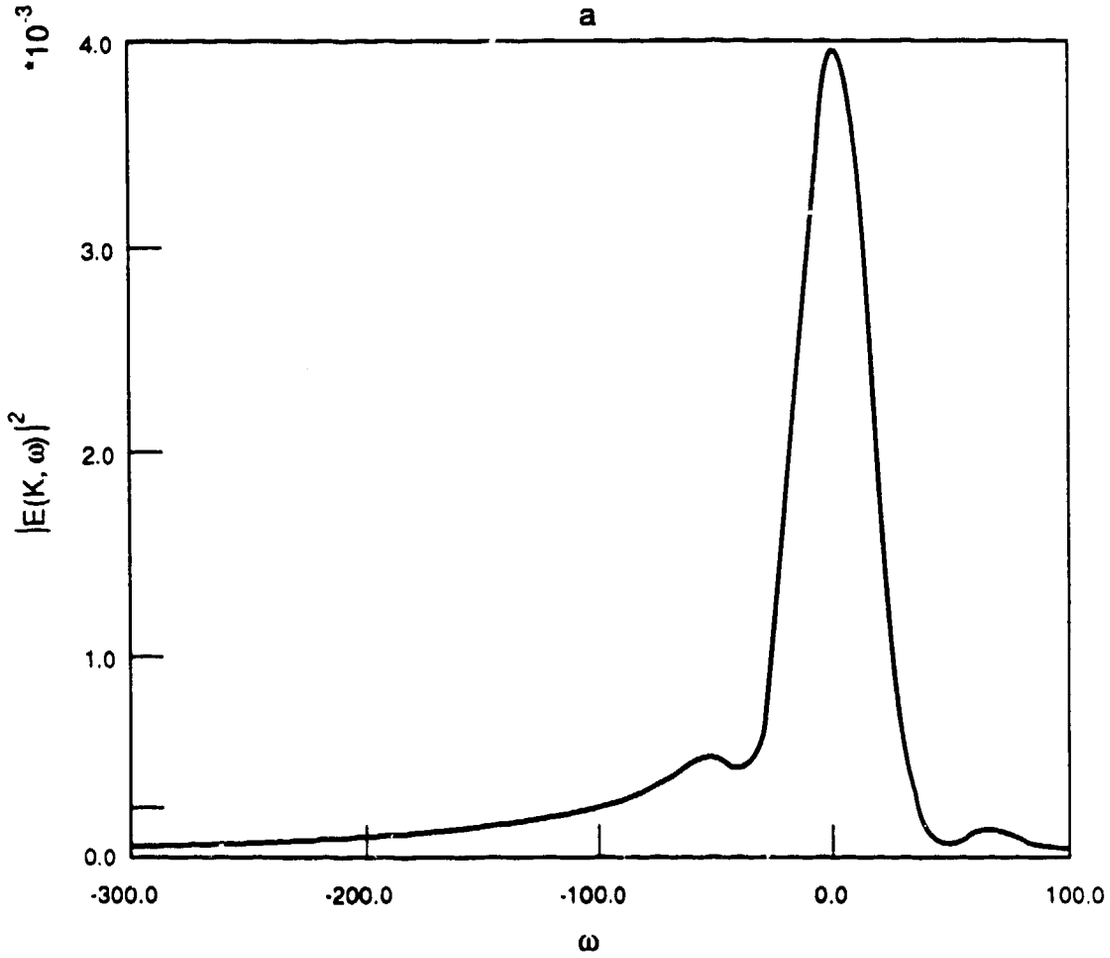
a
*10^-3
4.0
3.0
2.0
1.0
0.0
|E(K, ω)|^2
-300.0
-200.0
-100.0
0.0
100.0
ω

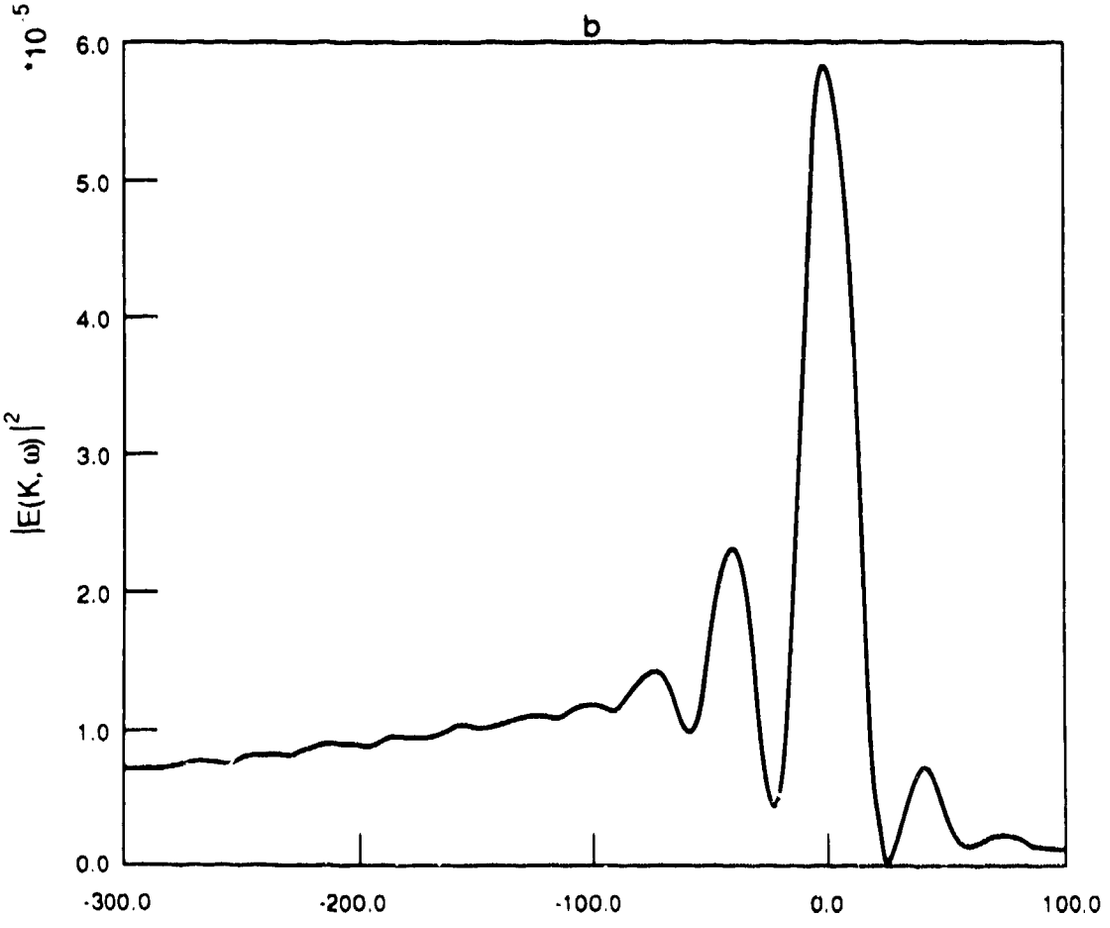
b
*10^-5
6.0
5.0
4.0
3.0
2.0
1.0
0.0
|E(K, ω)|^2
-300.0
-200.0
-100.0
0.0
100.0

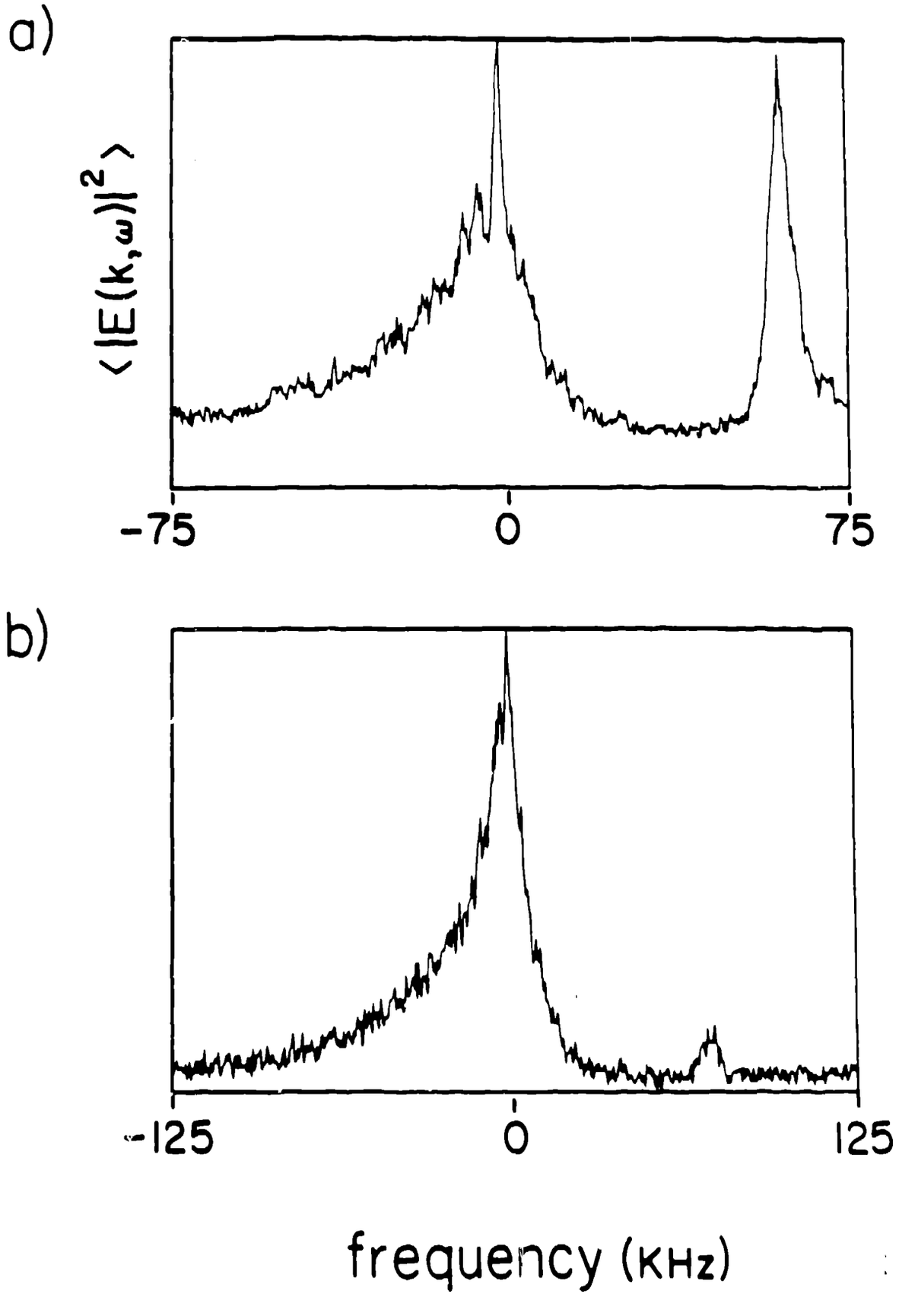
a)
$\langle |E(k,\omega)|^2 \rangle$
-75
0
75
b)
-125
0
125
frequency (KHz)

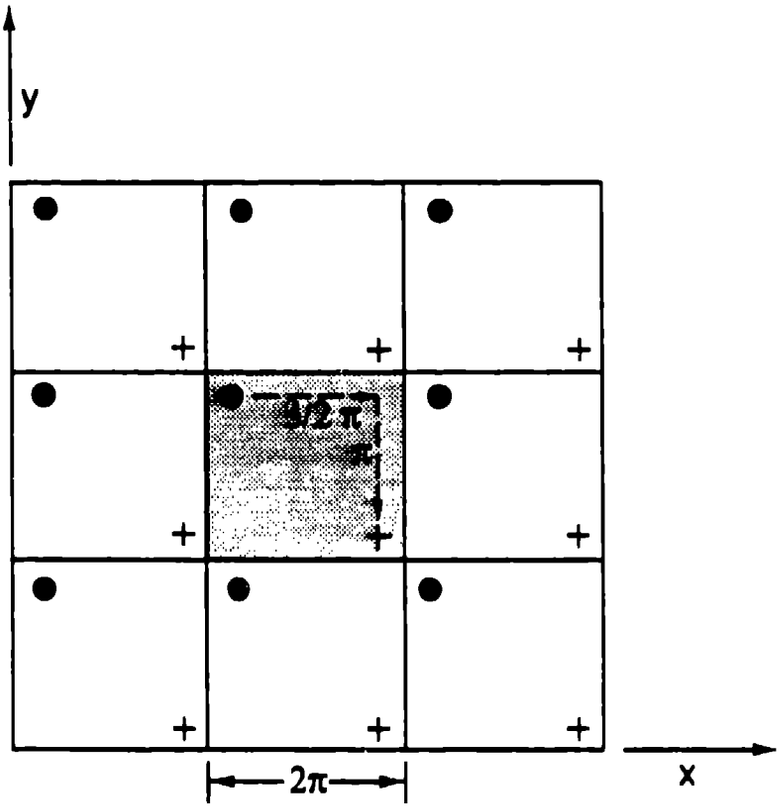
y
x
2π
π

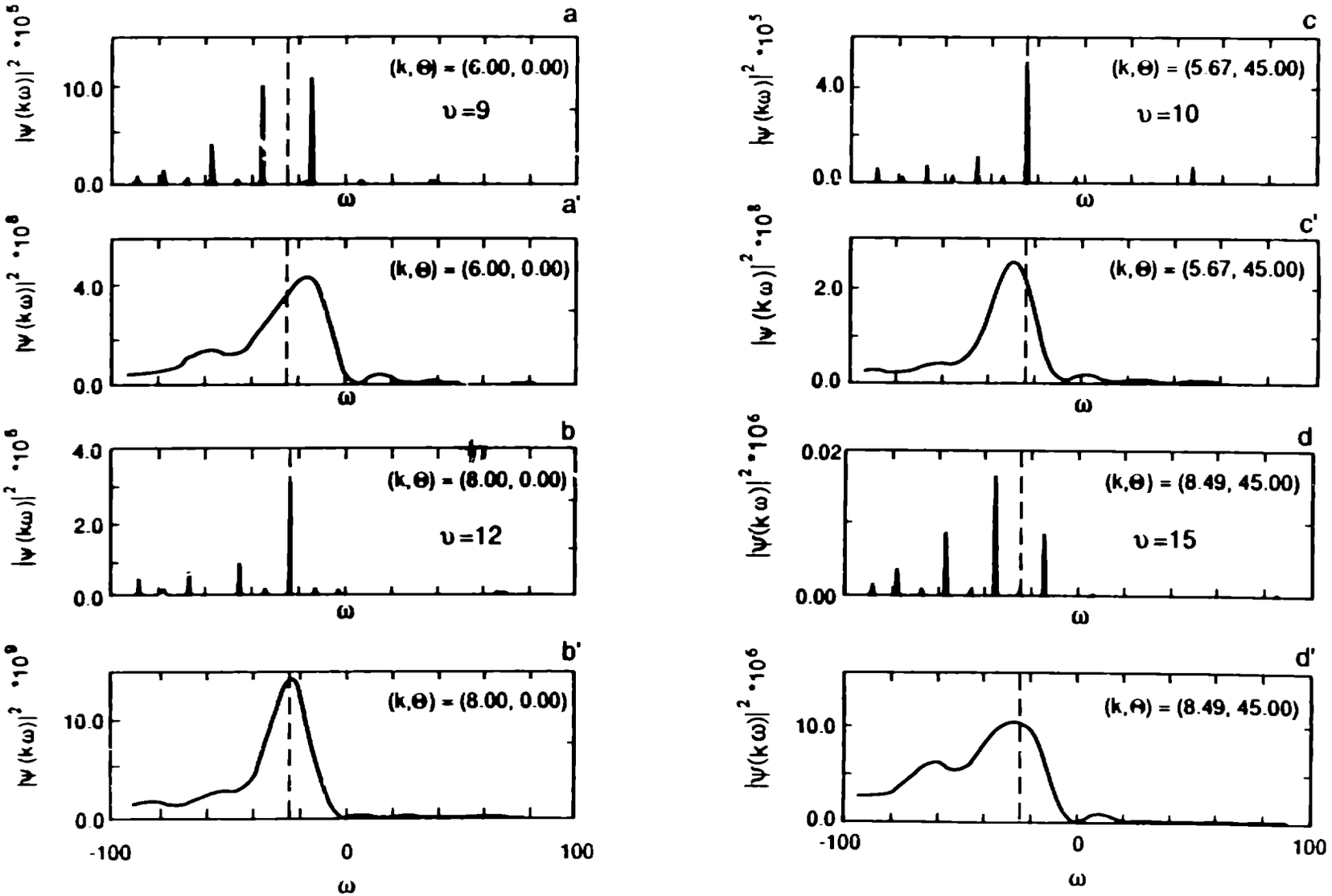
a
(k,Θ) = (6.00, 0.00)
υ=9
a'
(k,Θ) = (6.00, 0.00)
b
(k,Θ) = (8.00, 0.00)
υ=12
b'
(k,Θ) = (8.00, 0.00)
c
(k,Θ) = (5.67, 45.00)
υ=10
c'
(k,Θ) = (5.67, 45.00)
d
(k,Θ) = (8.49, 45.00)
υ=15
d'
(k,Θ) = (8.49, 45.00)
ω
-100
0
100

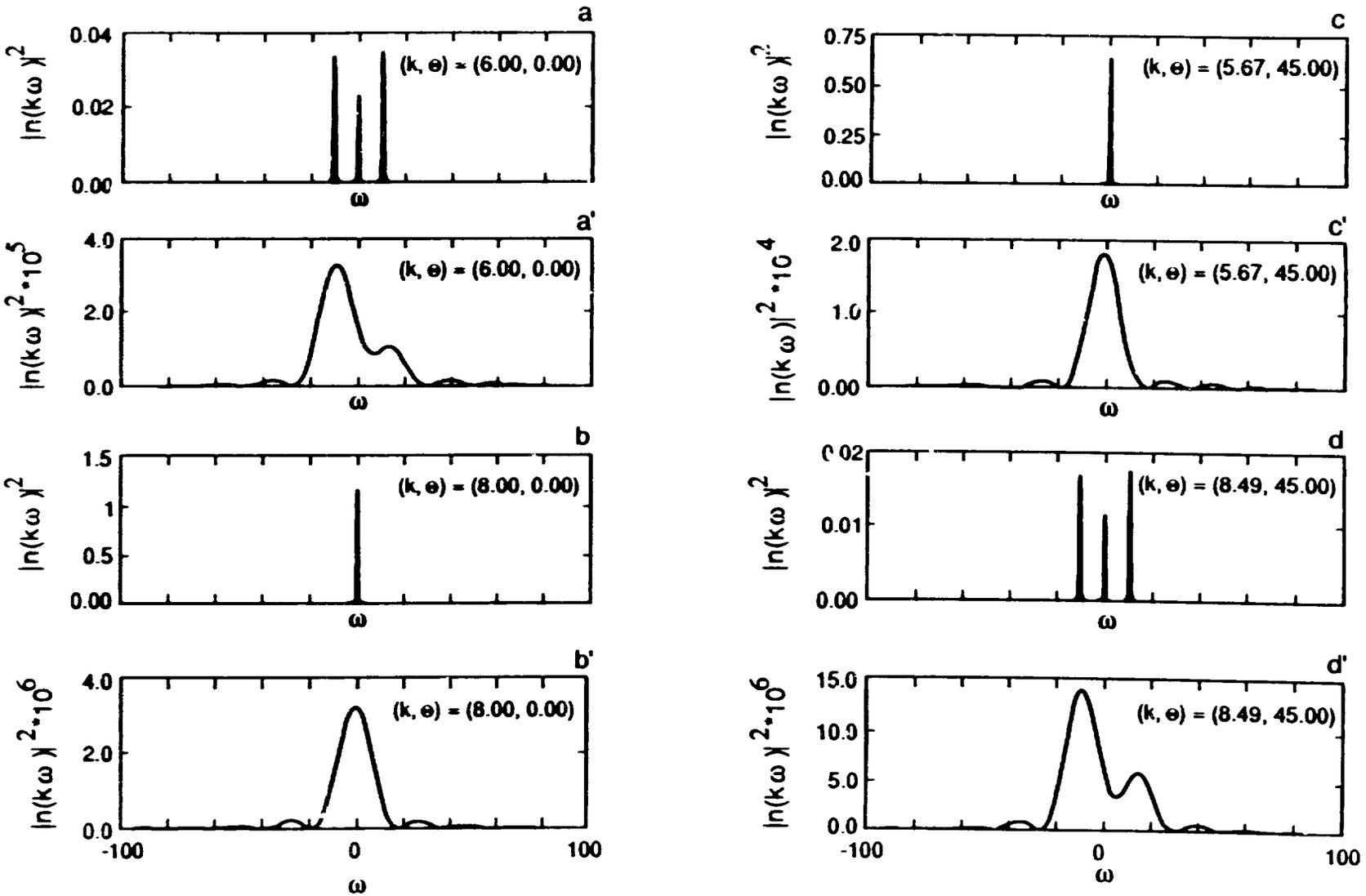
a
(k, θ) = (6.00, 0.00)
|n(kω)|^2
0.04
0.02
0.00
ω
a'
(k, θ) = (6.00, 0.00)
|n(kω)|^2 *10^5
4.0
2.0
0.0
ω
b
(k, θ) = (8.00, 0.00)
|n(kω)|^2
1.5
1
0.5
0.00
ω
b'
(k, θ) = (8.00, 0.00)
|n(kω)|^2 *10^6
4.0
2.0
0.0
-100
0
100
ω
c
(k, θ) = (5.67, 45.00)
|n(kω)|^2
0.75
0.50
0.25
0.00
ω
c'
(k, θ) = (5.67, 45.00)
|n(kω)|^2 *10^4
2.0
1.0
0.00
ω
d
(k, θ) = (8.49, 45.00)
|n(kω)|^2
0.02
0.01
0.00
ω
d'
(k, θ) = (8.49, 45.00)
|n(kω)|^2 *10^6
15.0
10.0
5.0
0.0
-100
0
100
ω